FRACTURE AND PERMEABILITY ANALYSIS OF THE SANTANA TUFF,

TRANS-PECOS TEXAS

APPROVED:

Supervisor:

Dr. John Sharp, Jr.

Dr. Dale Klein

Dr. Larry Lake

FRACTURE AND PERMEABILITY ANALYSIS OF THE SANTANA TUFF, TRANS-PECOS TEXAS

BY

CARLA MARIE MATHERNE (Fuller), B.S.

THESIS

Presented to the Faculty of the Graduate School of
The University of Texas at Austin
in Partial Fulfillment
of the Requirements
for the Degree of

MASTER OF ARTS

THE UNIVERSITY OF TEXAS AT AUSTIN

December 1990

note: Name change between completion of thesis and award of degree — degree awarded under Fuller

ACKNOWLEDGEMENTS

This research was performed under appointment to the Civilian Radioactive Waste Management Fellowship program administered by Oak Ridge Associated Universities for the U. S. Department of Energy.

I would also like to acknowledge the role of my family, friends, and of course, Jeff. Your support and encouragement in this endeavor made all the difference in the world.

To Jack Sharp, my supervisor, thanks for doing just that--supervising and guiding my work. I've learned quite a bit from you, and this thesis would not have been possible without your support.

Finally, I would like to thank everyone else who had a role in my research and education: Dr. Larry Lake and Dr. Dale Klein, my two committee members; Mr. Don Alexander and Mr. Kenneth Krupka, my supervisors at the Department of Energy; Mr. Dan Soeder of the Institute of Gas Technology; Dr. Wulf Gose of the Geology Department; and Dr. Chris Henry, of the Bureau of Economic Geology.

July, 1990

ABSTRACT

FRACTURE AND PERMEABILITY ANALYSIS OF THE SANTANA TUFF,

TRANS-PECOS TEXAS

BY

CARLA MARIE MATHERNE, B.S.

SUPERVISING PROFESSOR: DR. JOHN M. SHARP, JR

A fracture and permeability analysis was performed on the Santana Tuff because of its similarity to the Topopah Springs unit at the Yucca Mountain site. The Topopah Springs unit is the proposed horizon for the spent nuclear fuel repository. Because of the impossibility of completely characterizing the flow properties of the unit without destroying the characteristics that make it desirable as a repository, other ash flow tuffs must be studied. The Santana Tuff and the Topopah Springs tuff both are rhyolitic in composition, nonwelded to densely welded and fractured.

Fractures were examined at six outcrop locations spanning a five mile area. Stereonets and rose

diagrams were constructed from over 312 fracture orientations. Although the composite data showed two major orientations of nearly vertical fractures, fracture trends at individual outcrops showed a variety of preferred orientations.

Over 900 surface permeability measurements were taken using a mini-permeameter. The samples were categorized by three observed types of surface weathering: fresh, weathered, or varnished. Fracture surfaces were generally classified as weathered. The average permeabilities for the samples are 55.33 millidarcies, 5.03 millidarcies, and 3.31 millidarcies, respectively. The one-way statistical analysis performed on the data indicated that the permeability of fresh tuff surfaces is significantly different than both the permeabilities of the weathered and varnished tuffs, using both a least significant difference and greatest significant difference test. However, no difference was shown to exist between the weathered and varnished tuff permeabilities.

Samples of fresh, weathered, and varnished tuffs were examined by X-Ray Defraction, the Scanning Electron Microscope, and in thin section. The SEM analysis showed surface differences between the three

weathering classifications. The weathered and varnished samples were similar, exhibiting a platy, lamellate texture. The fresh surfaces were irregular and jagged. In thin section, a thin rind of dark minerals (FE-oxides) is observed on the edges of the varnished samples and in microcracks. This fills surface pores and causes the reduction in permeability. Two other zones of weathering have been identified in some of the samples, which may also cause changes in permeability.

Tuff permeabilities were also analyzed for directional dependence. After an ash flow tuff is deposited and cooled, it may undergo flattening of pumice fragments and glass shards. These flattened fragments can be identified in handsamples, and are indicative of the direction of flow emplacement. The analysis showed that permeability is enhanced parallel to the emplacement direction, which is generally horizontal. Cut surfaces showed a 30% decrease in permeability perpendicular to flow direction. On varnished surfaces, this trend is still evident, although decreased in magnitude. This is expected because of the clay particles which make up the desert varnish.

This study indicates that the formation of low permeability weathering rinds in association with vertical fractures may inhibit infiltration at the surface. It may accelerate infiltration at depth and allow more fluid to penetrate vertically into the tuff. In the event that fluid is absorbed into the matrix, it will travel horizontally, along the enhanced permeability parallel to the emplacement direction.

TABLE OF CONTENTS

LIST OF TABLES

LIST OF FIGURES

INTRODUCTION

This study is an attempt to illustrate fracture and permeability patterns of the Santana Tuff of Trans-Pecos Texas. The Santana is a vitric-crystal tuff and ranges from nonwelded to densely welded and fractured. These characteristics are typical of ash flow tuffs, and are important in understanding fluid flow through tuffs. This topic has become increasingly important because the present proposed location of the high level nuclear waste repository is in a tuff at the Yucca Mountain site in Nevada. Research is now being conducted on hydrologic properties of ash flow tuffs to insure that the site is capable of keeping the waste isolated from the accessible environment for up to 10,000 years.

The volcanic sequence at the Yucca Mountain site is about 6500 feet thick and the depth to the water table varies from 1700 feet to 2400 feet below land surface. The repository would be constructed in the Topopah Springs Member of the Paintbrush Tuff formation, in the unsaturated zone. The Topopah Springs Member is a compound cooling unit which is about 1100 feet thick at the site and thins abruptly to the south (Figure 1).

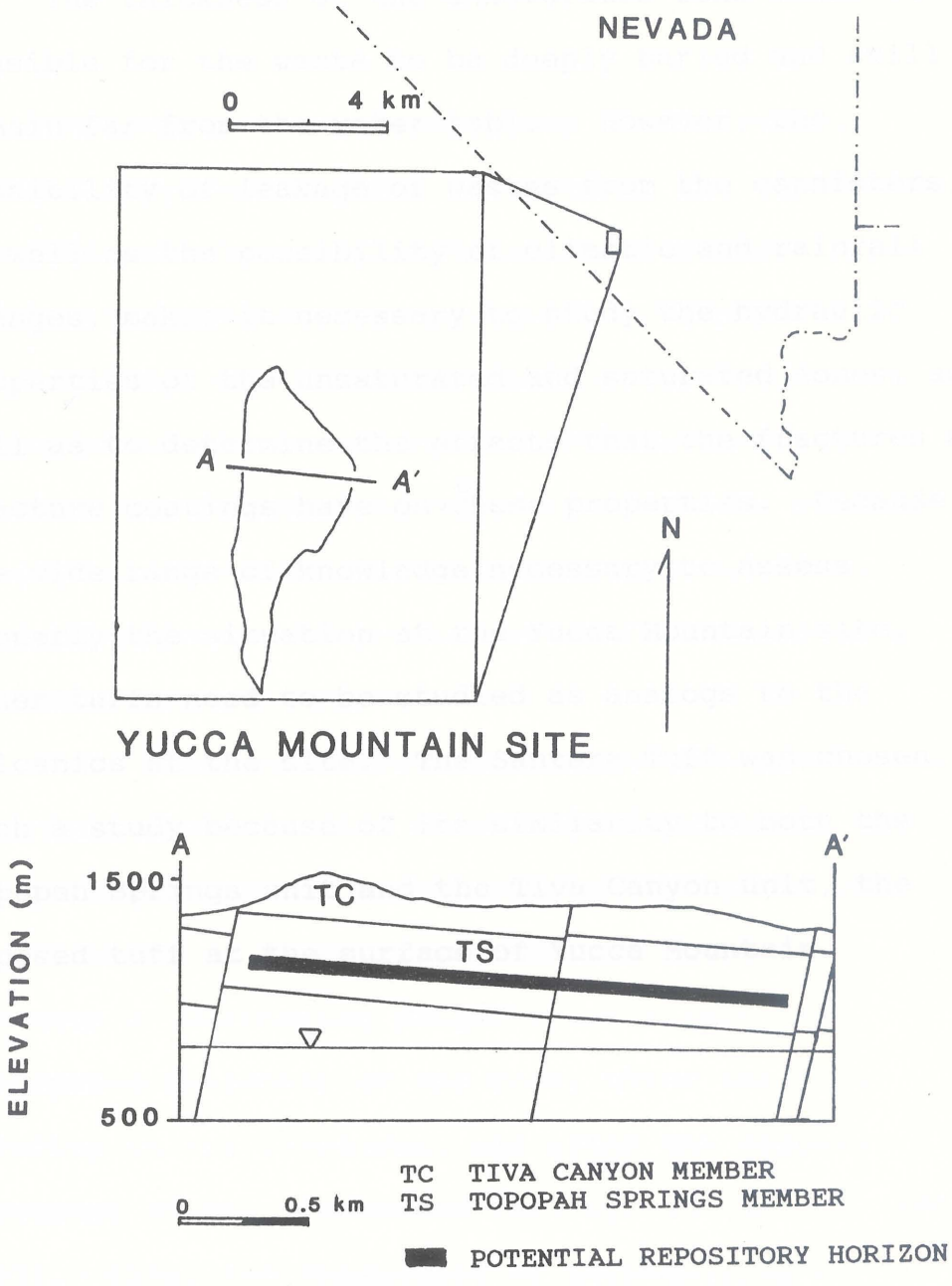

Figure 1: Proposed location of high level waste repository at the Yucca Mountain site, with a cross section showing the potential repository horizon.

The thickness of the unsaturated zone makes it possible for the waste to be deeply buried and still remain far from the water table. However, the possibility of leakage of wastes from the cannisters, as well as the possibility of climatic and rainfall changes, makes it necessary to study the hydraulic properties of the unsaturated and saturated zones, as well as to determine the effects that the fractures and fracture coatings have on these properties. Because of the wide range of knowledge necessary to assess properly the situation at the Yucca Mountain site, other tuffs need to be studied as analogs to the volcanics at the site. The Santana Tuff was chosen for such a study because of its similarity to both the Topopah Springs unit and the Tiva Canyon unit, the exposed tuff at the surface of Yucca Mountain.

OBJECTIVES

The objectives of this study are to evaluate the permeability and fracture patterns of the Santana Tuff, a welded ash flow tuff in Trans-Pecos Texas. Aspects of the fractures such as orientation, dip, connectivity, and spatial relations were studied to determine if there are any discernible patterns relating to distance and direction from the caldera, large scale faulting, or cooling. This knowledge may be applicable to the prediction of fracture dependent flow directions at depth.

Core plug and surface permeability measurements were taken to determine whether patterns exist which are dependent on the degree of weathering as well as to direction of flow emplacement and flattening. The presence of weathering products can affect the adsorptive character of the rock, alter the flow velocity in the fractures, and alter the dispersive character of the fractured rock system (Moench, 1984; 1983). Also, the dependence of permeability on direction of emplacement and flattening, can create enhanced flow paths for fluids once they are imbibed into the matrix.

STUDY AREA

This study was conducted on the Santana Tuff of Trans-Pecos Texas. The Santana Tuff is part of the Trans-Pecos volcanic field, and was deposited 26 - 27 million years ago. The field lies at the south-east end of the Basin and Range province, whose effects can be seen by large scale west-northwest trending faults. The Santana caldera is located in northern Mexico, where there are also extensive deposits of the Santana Tuff (Figure 2).

The Santana Tuff is a vitric crystal ash flow tuff almost entirely rhyolitic in composition. In places it may be as thick as 550 feet, and may be composed of 1 to 4 flows. Each flow generally shows a typical pattern of nonwelded zones at the top and bottom, grading into a central densely welded zone. Most of the nonwelded zones have been eroded away, exposing thick sequences of partially to densely welded, fractured tuff. The welded portions of the Santana tuff form mesas throughout the area. The mesas are generally separated by the Basin and Range faults.

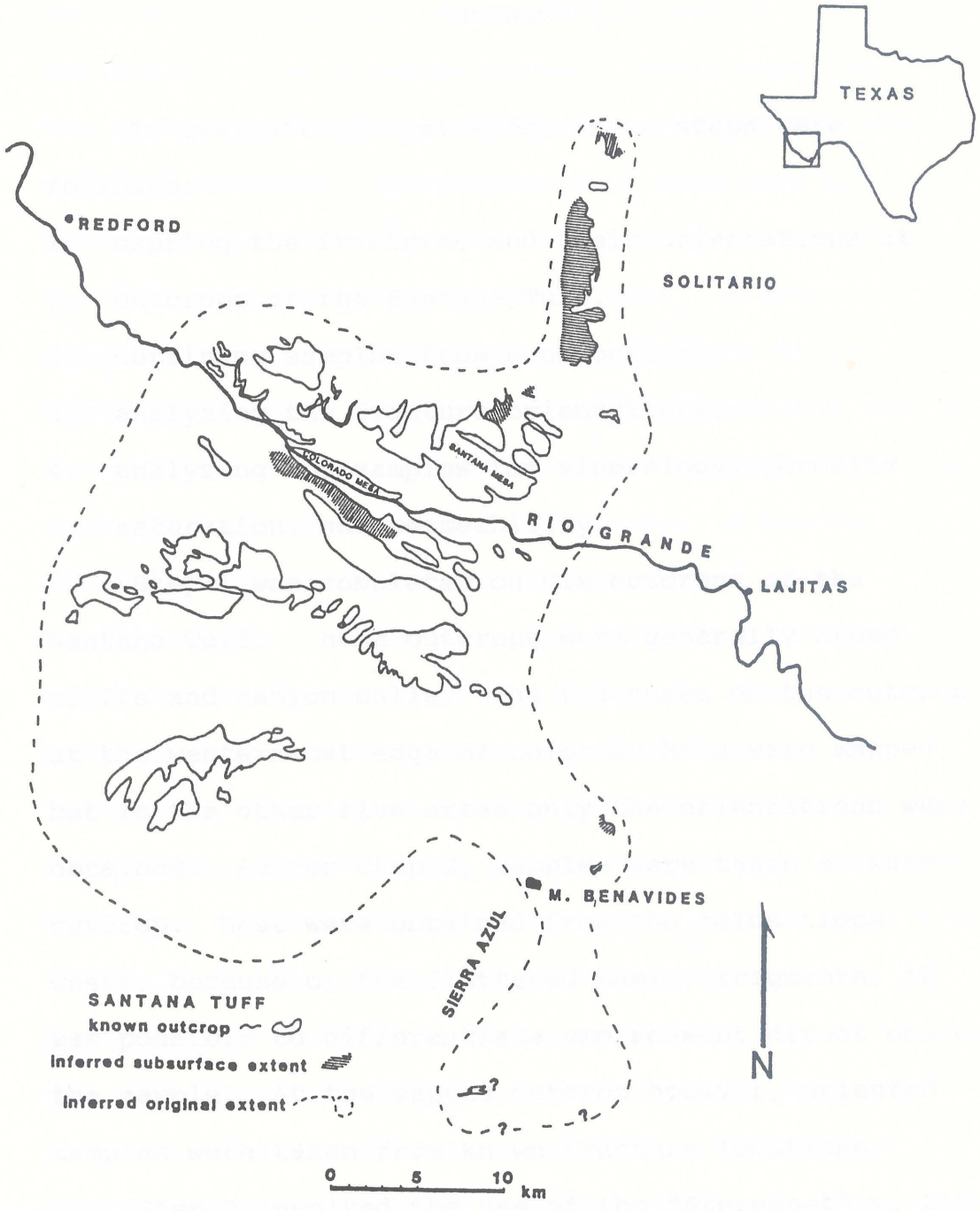

Figure 2: Inferred original extent of the Santana Tuff (modified from Gregory, 1981).

APPROACH

To evaluate the patterns, these steps were followed:

1. mapping the fractures and their orientations at outcrops of the Santana Tuff,
2. obtaining samples from each outcrop,
3. analyzing the fracture orientations,
4. analyzing the samples for mineralogy, porosity saturation, and permeability.

Step 1 was completed on six outcrops of the Santana Tuff. These outcrops were generally steep cliffs and canyon walls. The fractures on the outcrop at the westernmost edge of Colorado Mesa were mapped, but in the other five areas only the orientations were obtained. As per step 2, samples were taken at each outcrop. Most were obtained from the talus slope, where, because of the flattened pumice fragments, it was possible to differentiate emplacement directions on the sample. At the mapped outcrop however, oriented samples were taken from known fracture locations.

Step 3 involved the use of the "Stereonet" v. 2.9 (Allmendinger, 1987) program on a Macintosh computer. This computer program used the fracture orientation

data to plot rose diagrams and equal area stereonets of the poles to the fracture planes. These were made for the data on individual outcrops, as well as for the combined outcrops. Histograms were also made for the aperture orientations. These graphically show which aperture orientations are most common. Fracture connectivity was represented by the ratios of the three types of fracture terminations and interactions seen at the mapped outcrop. These include terminations in the rock matrix, crossings, and abutments. A fractal analysis was also performed on the mapped area.

Among the instruments used for step 4 are a gas permeameter (Institute of Gas Research, Chicago), a portable gas minipermeameter (developed in the University of Texas at Austin Petroleum Engineering department), the scanning electron microscope (SEM) and the x-ray diffractometer (XRD). Four samples were sent to the Institute of Gas Research to determine gas permeability, relative water permeability, saturation and porosity--thin sections were also made from the samples. The portable gas permeameter was used to measure permeabilities in grid patterns on cut surfaces as well as on fresh, weathered and varnished surfaces of the tuff samples. Over 1000 permeability

measurements were then run through a statistical package (Minitab) to determine the relationship between the fresh, weathered, and varnished samples. The XRD was used to determine mineralogical changes between the fresh, weathered, and varnished tuff surfaces.

BACKGROUND INFORMATION ON ASH FLOW TUFFS

PHYSICAL FEATURES OF ASH FLOW TUFFS

DEPOSITION

Ash flow tuffs are deposited as a result of a nuée ardente type of eruption. The turbulent mixing of gas and pyroclastic material causes the deposition of volcanic ash (Cook, 1960; Ross and Smith, 1961). As a result of this manner of deposition, ash flow tuffs are generally unstratified and poorly sorted. Thickness and areal extent of the tuffs depend on the amount of material erupted, as well as the topography over which it was emplaced (Winograd, 1971; Wood and Fernandez, 1988).

MINERALOGY

Tuff deposits primarily consist of glass shards, lithic fragments, pumice fragments, and phenocrysts. They are generally rhyolitic in composition, characterized by feldspar phenocrysts and polymorphs of quartz. Biotite may also be present, along with a few small opaques. The feldspar grains may be euhedral to subhedral, while the quartz phenocrysts are more likely

to be rounded and embayed (Ross and Smith, 1961; Barker, 1983).

Lapilli, pumice fragments 4 to 32 mm in size, are generally found near the top of a flow. Lithic fragments are incorporated into the flow from the underlying terrain (Ross and Smith, 1961). The glass shards, which make up the groundmass, are composed of amorphous silica which may crystallize as cooling progresses.

WELDING

Welding, the process of cohesion of glassy fragments, causes deformation of both pumice fragments and glass shards. Usually three transitional zones of welding are present in tuff formations: zones of no welding, partial welding, and dense welding (Ross and Smith, 1961). The degree of welding is controlled by temperature, amount and composition of volatiles, composition of ash, lithostatic load, rate of cooling, and rate of crystallization (Winograd, 1971).

Zones of no welding tend to occur at the top and bottom of a flow, but are dependent on the temperature and thickness of the flow. These zones show little deformation or loss of porosity because of compaction,

and are easily eroded. Partially welded zones exhibit a great diversity in texture, porosity, and degree of deformation of particles, and are usually best developed in cooler flows. Dense welding usually occurs in the center of a flow because it is the zone of greatest conservation of heat. This is also the zone of greatest porosity loss, jointing, and deformation/flattening of pumice fragments (Figure 3)(Peterson, 1979).

Sometimes pumice fragments may dissolve, or trapped volcanic gas can form cavities called miariolitic cavities, or lithophysae. These may or may not deform during welding. Welded tuffs will usually have a foliate (eutaxitic) structure because of the parallel arrangement of flattened plates, glass shards and pumice fragments (Figure 4). This flattening is indicative of flow direction. Lineations may occur by stretching of the cooling, but still plastic, material. Overall, welding causes a reduction in matrix porosity, but an increase in fracture porosity; it will also affect the type of recrystallization that can occur.

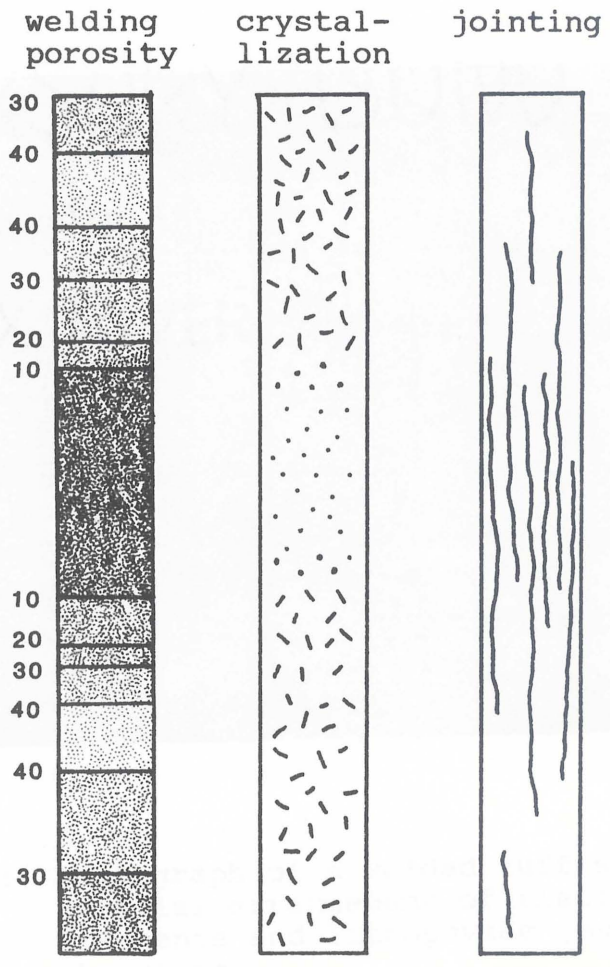

Figure 3: Sample section showing the relationship between degree of welding (percent porosity shaded), crystallization (vapor-phase mineralization dashed, devitrification dotted), and density of joints (modified from Smith and Bailey, 1966).

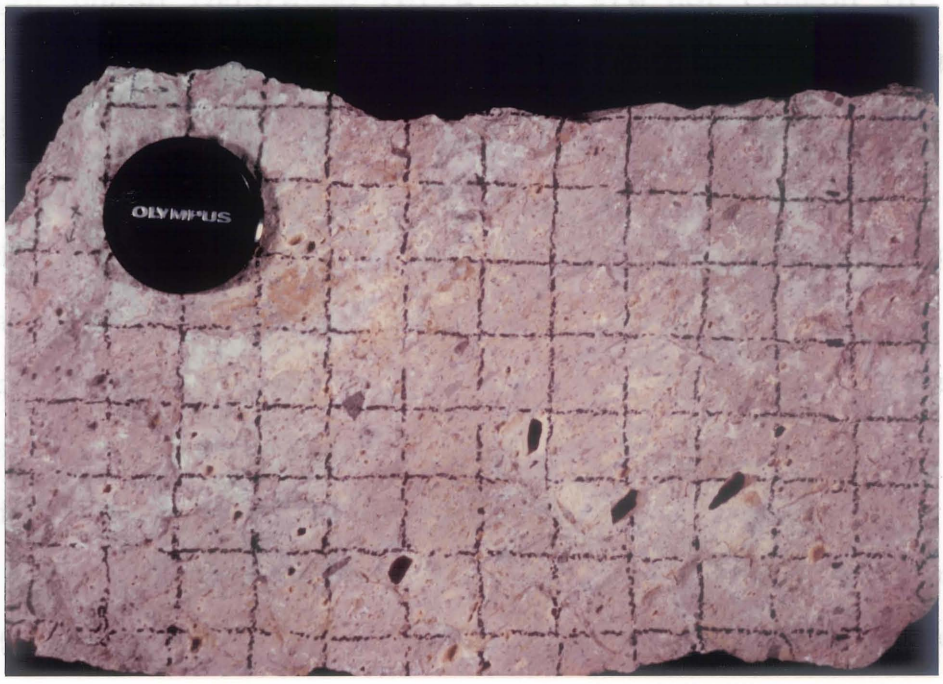

Figure 4: Photograph of a welded tuff showing the parallel arrangement of flattened pumice fragments and lithophysae (eutaxitic structure).

JOINTING

Joints in tuffs are commonly caused by the shrinkage of glass shards as they weld together and cool. They are best developed in welded tuffs and vapor phase indurated tuffs, and are not common in nonwelded, noncrystallized tuffs. Ragan and Sheridan (1972) found that joint spacing varies from a few inches to a few feet, depending on the cooling rate, thickness, and degree of welding. Columnar jointing is the most common type of jointing found in volcanic rocks. They form as networks of interconnected tension fractures with large length to diameter ratios (Figure 5) (Degraff and Aydin, 1987).

Low angle fractures may also be seen in ash flow tuffs. They are believed to form as the flow degases and collapses while it is still undergoing horizontal movement (Wood and Fernandez, 1988).

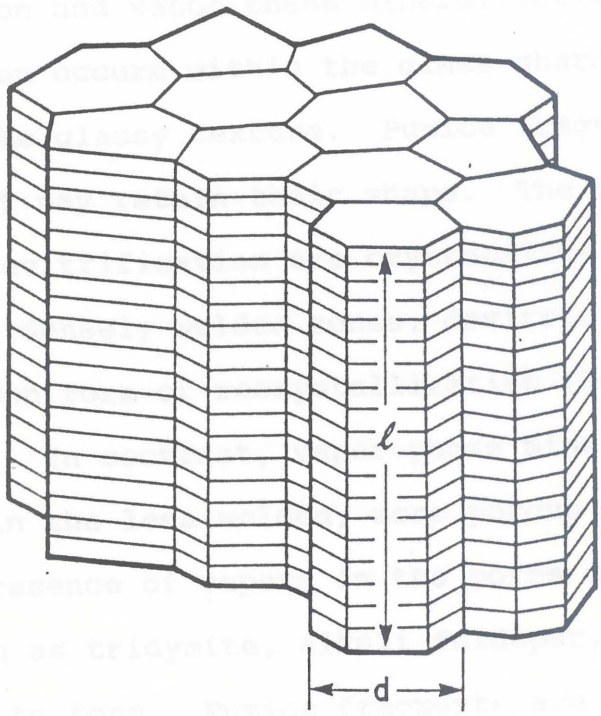

Figure 5: Basic geometry of columnar joints: idealized vertical columns with horizontal bands on joint surfaces. Symbols represent column length (ℓ), column diameter (d).

RECRYSTALLIZATION

Recrystallization occurs in two ways: devitrification and vapor phase mineralization. Devitrification occurs within the glass shards and obliterates the glassy texture. Pumice fragments also devitrify, but may retain their shape. The dominant products of devitrification are crystobalite and feldspar. In densely welded zones, devitrification is the most common form of recrystallization (Ross and Smith, 1961). In contrast, vapor-phase mineralization takes place in the less welded, more porous parts of a flow. The presence of vapors in the pores cause minerals such as tridymite, alkali feldspar, and crystobalite to form. Pumice fragments are especially susceptible to vapor phase mineralization, as they have much entrapped gas. Vapor phase mineralization tends to clog pores, thus decreasing porosity and permeability (Smith, 1960).

POST-COOLING ALTERATION

There are three types of post cooling alterations which tend to block open pores and fracture surfaces: zeolitization, devitrification, and desert varnish. Zeolitization is a low temperature, low pressure alteration of volcanic glass, which forms clay minerals (Berry, et al., 1985). Deuteric alteration works on the mafic minerals, causing them to form oxides or small opaque minerals (Barker, 1983). These two usually occur within the rock matrix. Desert or rock varnish, is found on the surface of rocks.

Desert varnish is a thin accretion of Mn-Fe oxides, clay particles and trace elements (Dorn, 1986). It is formed as microorganisms oxidize ambient manganese and iron (Krumbein and Jens, 1981; Dorn and Oberlander, 1982; Taylor-George, et al, 1983). These oxides are then mixed with the clay minerals that settle onto the rock surfaces. Varnish growth is limited by the amount of airborne clay particles and the rate of microbial oxidation (Dorn, 1986). The color of varnishes can range from orange to black, depending on the relative concentrations of manganese and iron. The manganese-poor varnishes are orange, and occur in deserts where the rock surfaces are in direct

contact with alkaline material. Black varnishes are, in turn, manganese-rich (Dorn, 1984).

Dorn (1986) proposed a model for varnish micromorphologies, where there is a continuum of forms which vary from botryoidal to lamellate (Figure 6). These micromorphologies can be correlated to the amount of vegetative cover. Botryoidal varnish is found in areas where vegetative cover is 40-50% and wind-blown clay particles are relatively sparse, while lamellate and intermediate varnish can be found in areas from 5 to 35% vegetation. Where there is little vegetative cover, the dust particles can readily settle onto the rock surface to form the lamellate structure. The lack of clay particles, in addition to vegetation, allows the oxides to cluster around the microbial nuclei and form the botryoidal texture.

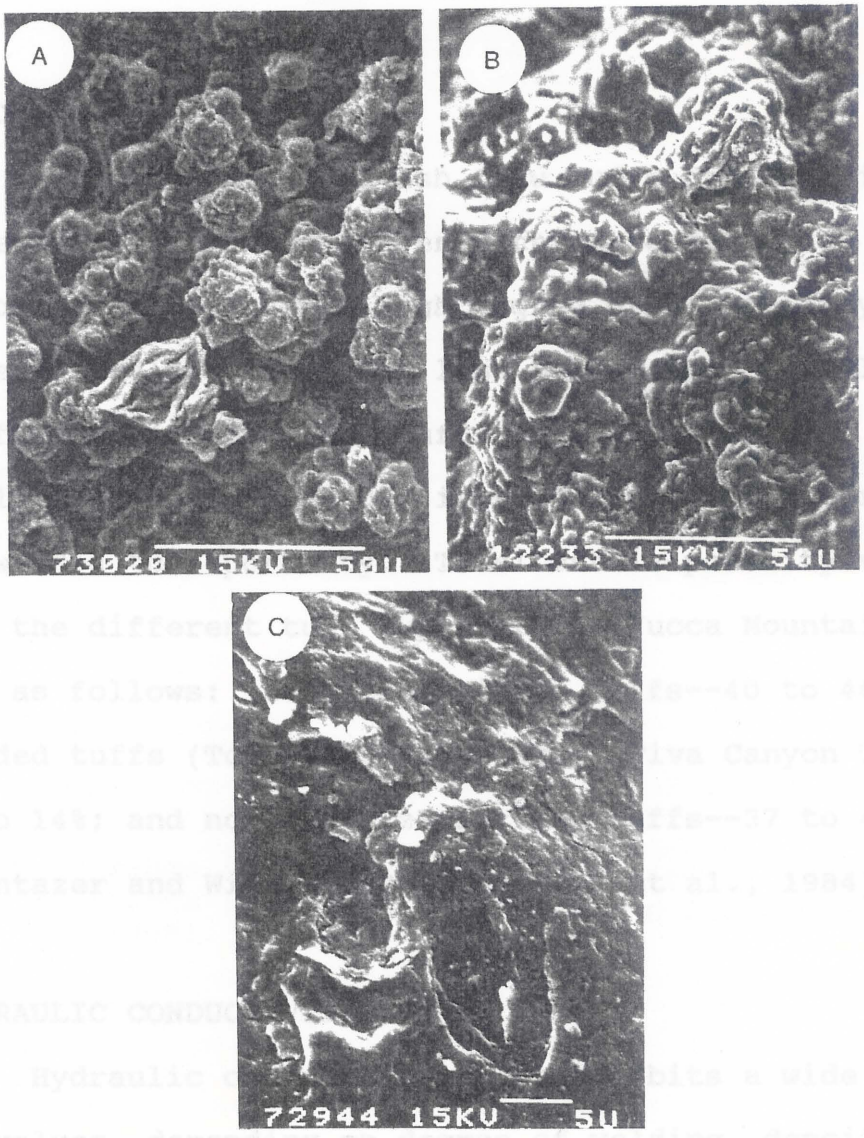

Figure 6: Micromorphology continuum: A. Botryoidal, B. Semi-botryoidal, and C. Lamellate micromorphology (Dorn, 1986).

HYDRAULIC PROPERTIES OF ASH FLOW TUFFS

PHYSICAL VALUES

POROSITY

Porosity values of ash flow tuffs can exhibit a wide range of values. Even within the same flow unit, porosity values show a high degree of variability. In general, welded tuffs are less porous than nonwelded tuffs; and of nonwelded tuffs, the porosity of zeolitized nonwelded tuff is much lower than vitric nonwelded tuff porosity. Total matrix porosity values for the different tuff types at the Yucca Mountain site are as follows: nonwelded vitric tuffs--40 to 46%; welded tuffs (Topopah Springs Tuff, Tiva Canyon Tuff)--8 to 14%; and nonwelded zeolitized tuffs--37 to 46% (Montazer and Wilson, 1984; Peters, et al., 1984).

HYDRAULIC CONDUCTIVITY

Hydraulic conductivity also exhibits a wide range of values, depending on degree of welding, density of fractures, degree of saturation and type of alteration. Figure 7 shows the ranges in hydraulic conductivity values from lab and field tests of the Nevada Test Site

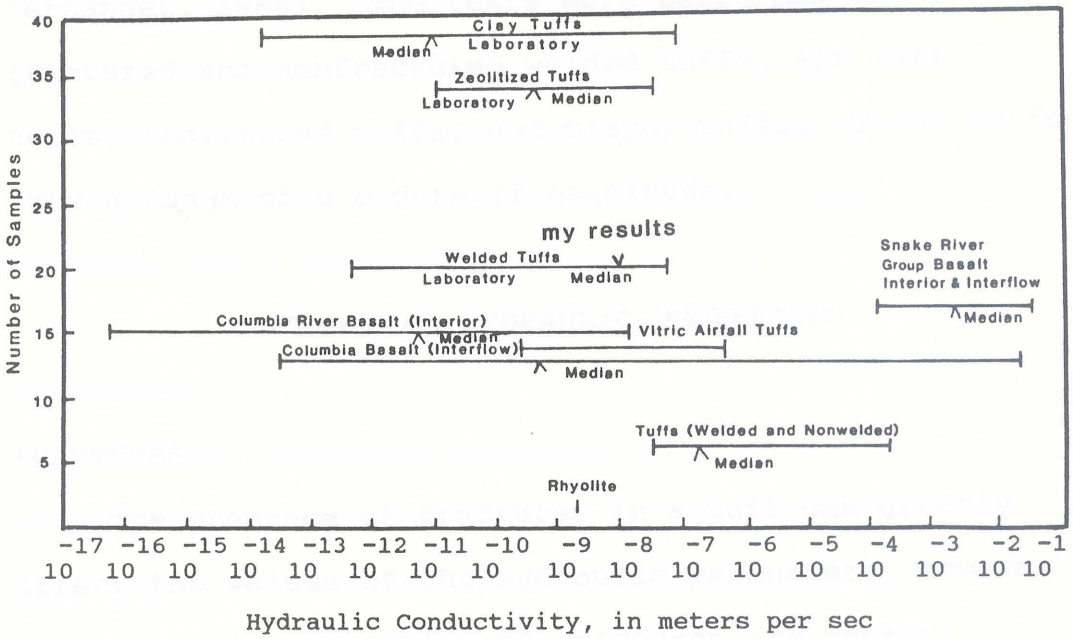

Figure 7: Range in hydraulic conductivity of volcanic rocks (modified from Wood and Fernandez, 1988).

(Winograd et al., 1975; Thordarson, 1983; Wood and Fernandez, 1988). The tests were performed on fractured and nonfractured welded tuffs, air fall tuffs, zeolitized tuffs, and clayey tuffs. These tuffs show a range of 8 orders of magnitude.

CONTROLS ON HYDRAULIC PROPERTIES

FRACTURES

The presence of fractures in a tuff can greatly affect the values of the hydraulic parameters, however the hydraulic properties of fractures are poorly understood. For the effects of fractures to be understood, model development must account for problems such as orientation, aperture and aperture orientation, connectivity, surface roughness and spatial distribution. The fractal geometry method may quantitatively describe fracture networks. Fractal analysis can show scale dependence or independence, and directional flow isotropy or anisotropy (Barton and Larsen, 1985; Barton and Hseih, 1989). Some transport models attempt to treat fractured media either as a continuum, or as a discrete representation of the fractured network (Long, et al., 1982; Schwartz, et

al., 1983). Others may take into account the fact that fractures are not smooth walled, parallel plate surfaces (Neuzil and Tracy, 1981). Finally, there are methods of mapping channeling of flow through the fractures, depending on surface roughness and aperture (Bourke, 1987, Neretnieks, 1987).

SATURATION

Another important determinant of hydraulic parameters in an ash flow tuff is the degree of saturation, because the mechanisms which govern fluid flow through the fractures and matrix change as the tuff moves from a saturated to an unsaturated state (Mualem, 1976; Duguid and Lee, 1977; Klavetter, 1984; Montazer and Wilson, 1984; Peters, et al., 1984; Sinnock, et al., 1984; Waddell et al., 1984; Wang and Narasimham, 1984; Peters and Klavetter, 1988). This change in behavior can be explained by capillary theory, which relates pore size and degree of saturation to the suction head. When the matrix is partially saturated, the fluid pressure in the water phase is less than atmospheric pressure. This pressure causes large pores to desaturate before the smaller ones. Therefore only those pores or fractures with a

small enough diameter or aperture for the radius of curvature of water to form will remain saturated--forming a capillary barrier (Figure 8). The fractures essentially remain dry because their apertures are one to two orders of magnitude greater than the average pore space, and higher capillary suction in the matrix pulls water from the fracture.

In cases where a fracture has a large asperity that brings it in close contact with the adjacent wall, residual water may collect (Figure 9). The hydraulic conductivity for the fracture in the plane of the fracture is near zero because these islands of water are discontinuous, and the air phase prevents water from flowing through the fracture. However, there is hydraulic conductivity across the fractures into the matrix (Figure 10). Therefore, at a low degree of saturation, most of the water movement is through the matrix, and the fracture conductivity is minor compared with that of the matrix.

However, as the matrix saturation increases, the fracture saturation increases nonlinearly. The islands of water grow and enable more water to be channeled from one matrix block to the other, until the islands coalesce and the fractures fill with water. At this

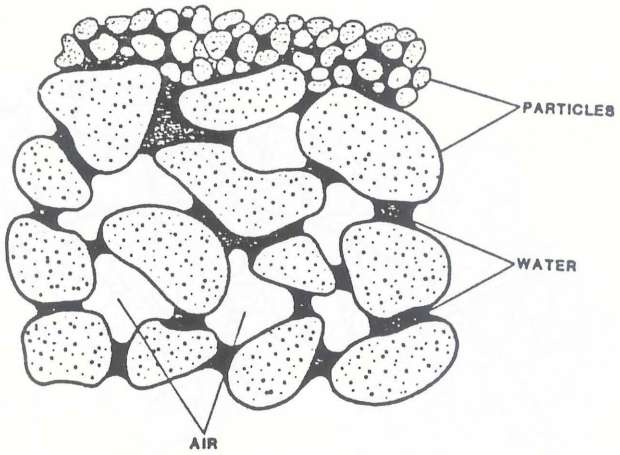

Figure 8: Sketch of a fine-grained layer overlying a coarse-grained layer, illustrating a natural capillary barrier (Klavetter, 1984).

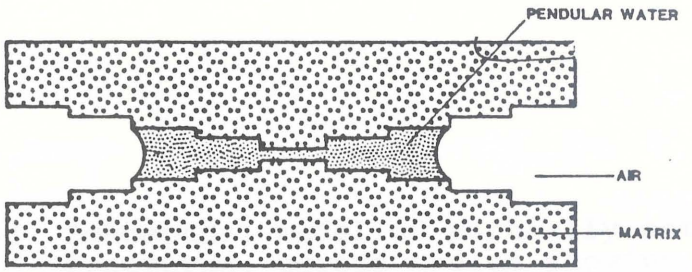

Figure 9: Sketch of pendular (residual) water collected near an asperity (modified from Klavetter, 1984).

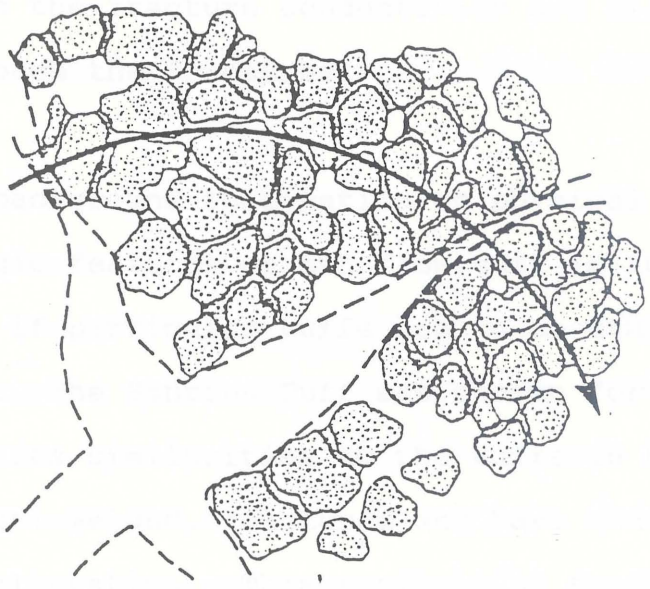

Figure 10: Conceptual model of partially saturated, fractured, porous medium showing schematically the flow lines moving around the dry portions of the fractures (Wang and Narasimhan, 1984).

point, the matrix hydraulic conductivity is negligible compared to the fracture conductivity and all flow occurs through the fractures.

This background information on physical and hydrogeologic features of ash flow tuff is important to understand if particular tuffs are to be studied and understood. The Santana Tuff was chosen for this study because of its similarities to the tuffs in Nevada. The tuffs are welded, fractured and have undergone some degree of alteration. This analysis of fracture and permeability patterns of the Santana Tuff may be analogous to the fracture and permeability patterns in the Topopah Springs tuff.

SANTANA TUFF

PHYSICAL FEATURES OF THE SANTANA TUFF

LOCATION

The Santana Tuff is a rhyolitic ash flow tuff located in Trans-Pecos Texas and northern Mexico. It has been studied by Maxwell and Dietrich (1970); McKnight (1968, 1970); Chuchula (1981); and Gregory (1981). Maxwell and Dietrich (1970) did the initial work on the Santana, and named the type locality. McKnight (1970) mapped the Santana and studied the composition of the tuff. Chuchula (1981) and Gregory (1981) studied the Santana in Mexico (Figure 11).

VEGETATION AND CLIMATE

The region is arid to semiarid, and is part of the Chihuahua Desert. Average rainfall is about 10 in/year generally occurring in late summer and early fall. The vegetation is typical of southwest desert regions, including cactus, catclaw, ocotillo, mesquite, creosote bush, and grasses. Vegetation is sparse because of lack of rain as well as lack of soil. Along the Rio Grande River cottonwoods and salt cedar may be found.

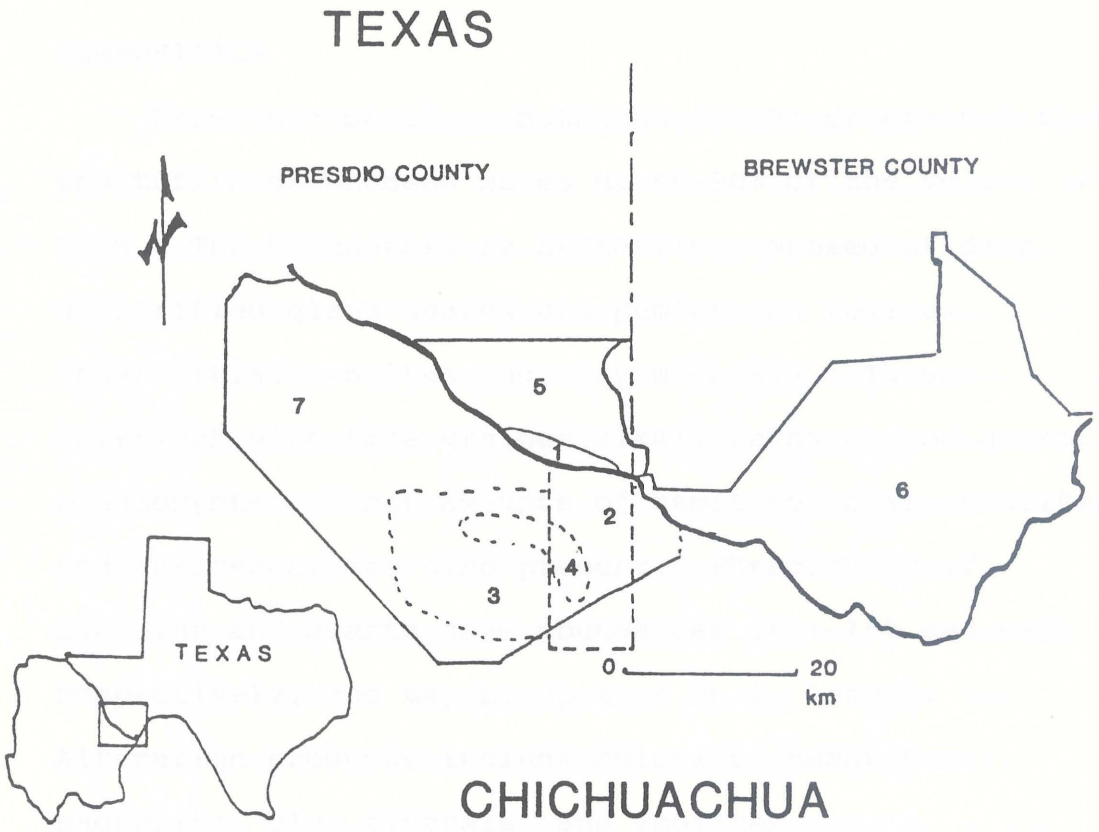

AREA		REFERENCE
1.	Santana Tuff	Matherne, this report
2.	Manuel Benavides	Gregory, 1981
3.	Sierra Rica Area	Chuchla, 1981
4.	San Carlos Skarn	Immitt, 1981
5.	Bofecillos Mountains	McKnight, 1968, 1970
6.	Big Bend National Park	Maxwell, et al., 1967
7.	Ojinaga-San Carlos Area	Arenal, 1964; Wolleben, 1966

Figure 11: Map showing previous studies of the Santana Tuff (modified from Gregory, 1981).

COMPOSITION

From thin section, McKnight (1968) determined that the tuff's groundmass makes up 60-90% of the volume of rock. The groundmass is primarily composed of dark, devitrified glass shards and pumice, as well as interstitial zeolites and clay minerals. These interlock with fine grained alkali feldspar and quartz phenocrysts. Minor amounts of hematite, opal, zeolites and chalcedony are also present. Phenocrysts of sanidine and quartz have abundances of 1-15% and 0-5%, respectively, and may be up to 4 mm in length. Alteration products include chlorite, hematite, magnetite, clay minerals, and zeolites.

WELDING

North of the Rio Grande River the Santana Tuff is divided into units of about 100 feet of thickness. When the Santana is less than 100 feet thick, it usually occurs as a single cooling unit and flow. In these sites the basal zone is nonwelded and ranges from a few centimeters to a few meters, and may grade into a vapor-phase nonwelded zone. The nonwelded zones, where present, are dull, friable, porous, and grey-buff colored, with interstitial zeolites and clay minerals. Where vapor-phase mineralization occurred, the tuff is indurated and displays deuteric alteration of mafic minerals. Then, depending on total thickness, a zone of moderate welding occurs 10 to 20 feet above the base. In the center of this moderate welding, a densely welded zone may exist, exhibiting a eutaxitic structure. Topping the sequence is a 20 to 50 feet thick nonwelded, vapor phase zone, much like the basal unit (McKnight, 1968; Maxwell and Dietrich, 1970).

Where the Santana Tuff is thickest, it may be composed of several compound cooling units. Each unit has alternating layers of nonwelding, slight welding, moderate welding, and intense welding, which grade into each other. The Santana is thickest in the south

central Texas area, where as many as six flows are seen in two cooling units (McKnight, 1968; Maxwell and Dietrich, 1970).

However, because the nonwelded zones and some of the partially welded zones are very friable and porous, they are usually eroded away. Most of the exposed Santana is the densely welded, fractured portion (McKnight, 1968). These include multiple flows of several hundred feet.

JOINTING

All outcrops of the Santana Tuff exhibit jointing, because they are, in general, the welded portions of the tuff. From a distance the outcrops appear to be columnar jointed, but closer inspection shows that they do not exhibit the 'typical' pattern shown in Figure 5 (Degraff and Aydin, 1988). Also, on cliffs where more than one flow can be seen, the jointing appears to cross flow boundaries (Figure 12).

Figure 12: Photograph of the Santana Tuff taken across the Rio Grande from the Colorado Mesa, showing how fractures tend to cross flow boundaries.

VARNISH

Desert varnish is prevalent on outcrops of the Santana Tuff. In general it is orangish in color, giving the Santana its distinctive appearance (McKnight, 1970). However some outcrops do exhibit a blackish varnish. The varnish is present on the exposed surfaces, but not on surfaces within cracks or joints. These fracture surfaces do still exhibit weathering in the form of clay coatings.

HYDRAULIC PROPERTIES OF THE SANTANA TUFF

PERMEABILITY

Values for core plug porosity, saturation, and permeability of the Santana Tuff were obtained from the Institute for Gas Technology (Soeder, 1988). The tests were performed on four core plugs from sample 64(Figure 16, page 45), taken in various orientations. Three of the samples are oriented horizontally: 64-1, 64A-1, and 64B-3. Two of the samples, 64-1 and 64A-1, are taken along an east-west trend, which is roughly horizontally perpendicular to the direction of flow emplacement. Core 64B-3 is parallel to emplacement in the N-S direction, and 64C-2 is a vertical core,

perpendicular to emplacement. The permeability data in Table 1 show that the three cores perpendicular to emplacement are half as permeable as core 64B-3, which is oriented parallel to flow emplacement.

The permeability of 64B-3 decreases with increasing confining pressure, indicating that permeability may decrease at depth because of increasing overburden pressure. From water saturation experiments there appears to be a reduction in water permeability, perhaps because of the presence of swelling clays in the pores, which is supported by XRD analysis. After initial water saturation measurements were taken, two plugs were left saturated for either 2 or 24 hours, before water permeabilities were measured. There was a 10% decrease in the core saturation for 2 hours, and a 25% decrease in saturation after 24 hours (Soeder, 1989).

Table 1: Core plug data from the Institute for Gas Technology.

SAMPLE NUMBER	ORIENTATION	DRY GAS PERM	GAS PERM HI STRESS	% SATURATION	GAS PERM AFTER SAT
64-1	horizontal E-W	121.05	NA	66.3	29.73
64A-1	horizontal E-W	167.86	NA	73.4	10.25
64B-3	horizontal N-S	255.99	205.10	71.6	NA
64C-2	vertical	116.89	NA	69.0	NA

(permeability in millidarcies)

POROSITY

Effective dry porosity in these samples ranged from 27.4% to 29.3%, with an average of 28.33%. There was no significant difference between the porosities of horizontal or vertical cores, or cores which are parallel or perpendicular to flow.

SATURATION

Measurements of saturation were obtained from the cores after water imbibition into completely dry cores. Degree of saturation also does not appear to be dependent on direction of flow/flattening. The values range from 66.3 to 73.4%, with an average of 70.1%. In addition, an increase in saturation corresponds to a decrease in gas permeability.

RESULTS

FRACTURE ANALYSIS

Fracture orientations were obtained at six outcrops of the Santana Tuff. The fractures were measured in two ways. At five locations, orientations were obtained by traversing the outcrop face, which may cause a bias in favor of fractures perpendicular to the face. The fractures at the sixth outcrop were actually mapped. At all six outcrops, the fracture orientations were analyzed with stereonets and rose diagrams, as well as aperture orientation histograms. At one site, fracture connectivity was measured as a ratio of fracture terminations, crossings and abutments. A fractal analysis was performed as well.

FRACTURE AND APERTURE ORIENTATIONS

The fracture orientations were studied to determine if there is a discernable pattern of orientations from outcrop to outcrop, and if it related to deposition, cooling, or tectonic forces. Also, knowledge of fracture orientations is needed to determine directional permeability. Histograms of

fracture apertures were made by plotting the degree of dip and dip direction. They are plotted to show the main direction of fluid transport through a fracture dominated flow system. Orientations were measured in these locations from west to east: Tapado Canyon, Rancheros Canyon, Colorado Mesa 1,Colorado Mesa 2, Closed Canyon, and Madera Canyon (Figure 13).

At the Tapado Canyon site, the westernmost outcrop if the area, 42 fracture orientations were measured along an outcrop face striking at N54W. The rose diagram and stereonet are shown in Figure 14. Both figures indicate a somewhat random distribution of fracture strikes. Also, the strike of the outcrop face appears to have little bias over the fracture strikes. The histogram of aperture orientations for the Tapado Canyon network is also shown in Figure 14. About 80% of the fractures are near vertical with a dip between 80 and 90 degrees.

Forty fracture orientations were taken at the next site, Rancheros Canyon, along a face striking N65W. This set of fractures has a prominent fracture orientation a N10E-N40E, and a minor one running about parallel to the strike of the face (Figure 15). The histogram of aperture orientations shows that 80% of

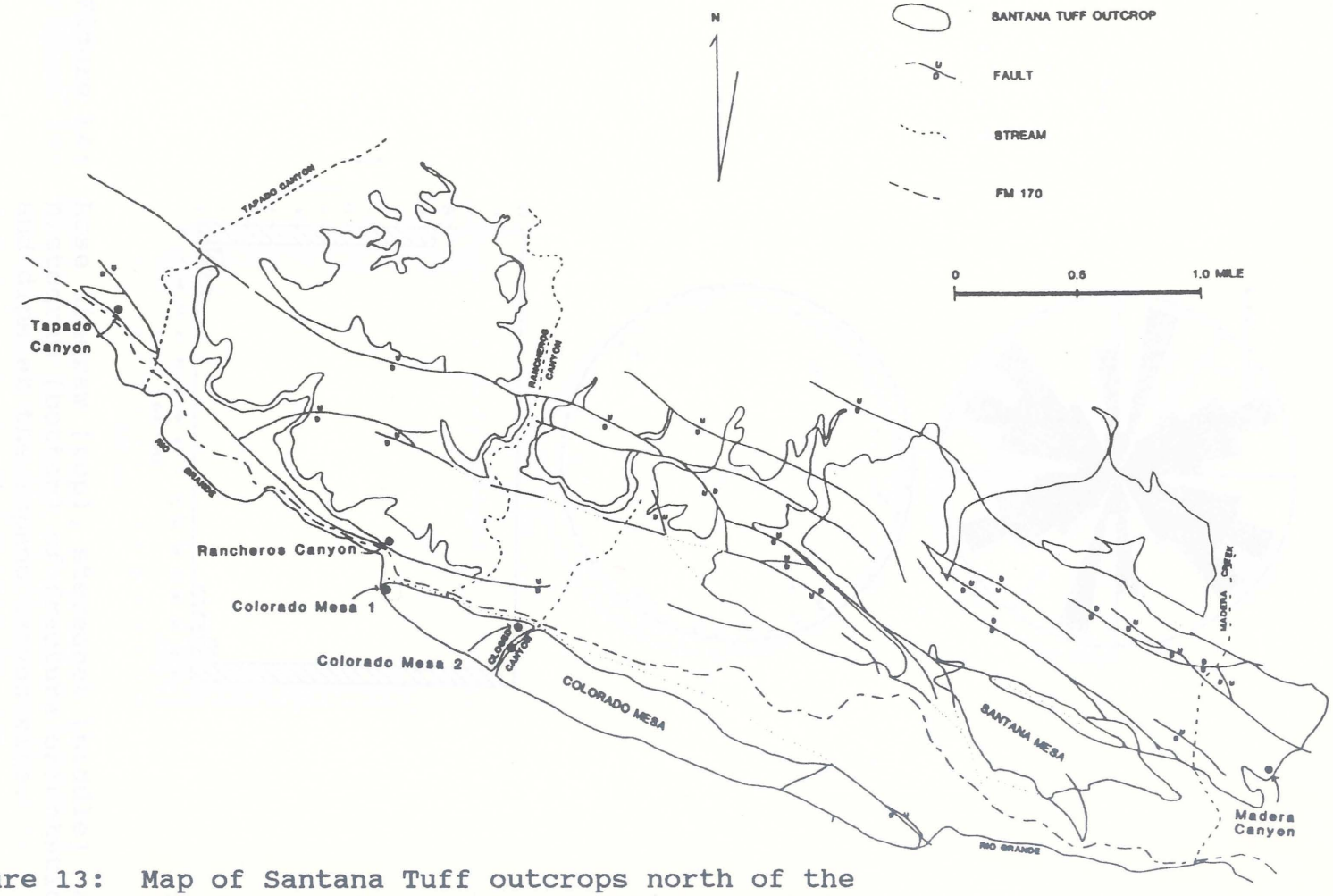

Figure 13: Map of Santana Tuff outcrops north of the Rio Grande with outcrop locations marked.

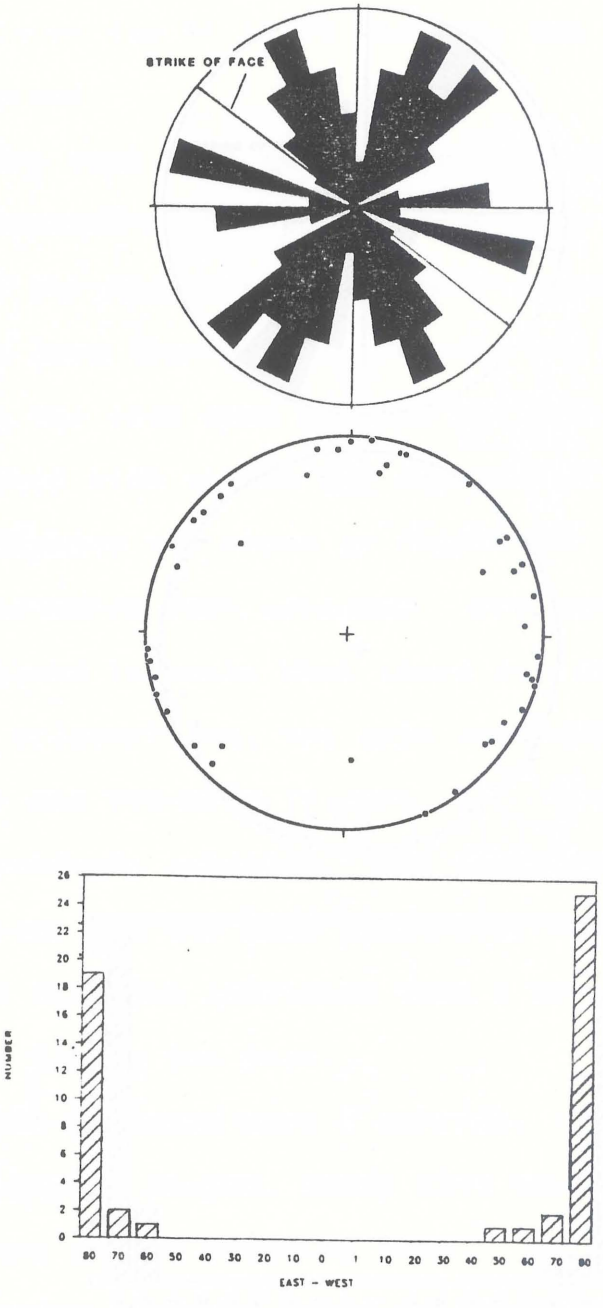

Figure 14: Rose diagram (top), stereonet (middle) and histogram (bottom) of fracture orientations and dips at the Tapado Canyon site.

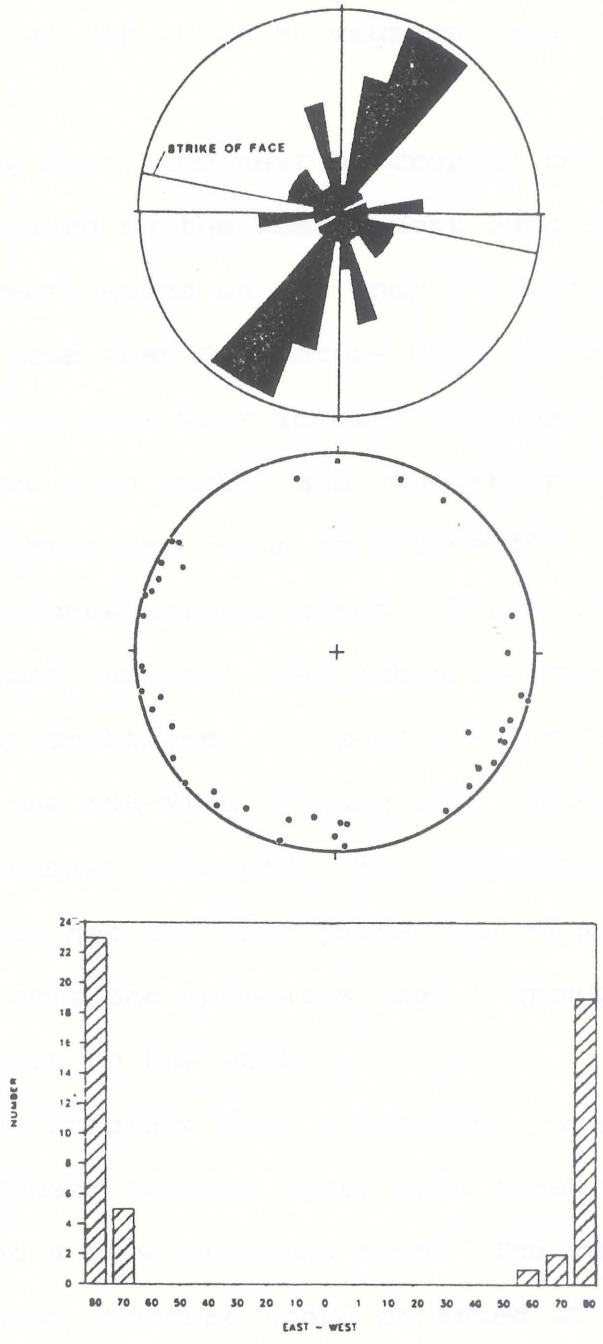

Figure 15: Rose diagram (top), stereonet (middle) and histogram (bottom) of fracture orientations and dips at the Rancheros Canyon site.

the fractures dip 80 to 90 degrees, and only 20% dip 70 to 80 degrees.

Moving east, the next outcrop is the Colorado Mesa 1 site, located on the westernmost edge of Colorado Mesa. It was mapped on a 1 inch = 1 meter scale. Any fractures less than 0.5 meters were not measured, cracks in the rock were ignored and some of the outcrop were covered with rubble and vegetation. The results of this mapping are shown in Figure 16. Orientations for 73 fractures were obtained. Stereonet and rose diagram plots indicate that there are two prominent fracture orientations, the main one located N70E-N90E, the minor one N0E-N10E (Figure 17). The fractures here are not randomly oriented. The histogram of aperture orientations has the same pattern of other plots in the area, but this one indicates that a greater number of fractures dip to the east.

At the Colorado Mesa 2 outcrop, located near the mouth of Closed Canyon, forty five measurements were taken along a face striking N80W. The rose diagram shows a major fracture trend oriented at N20E-N40E, and two minor trends at N10W-N20W and N80E-N90E (Figure 18). The histogram of aperture orientations shows that the fractures are nearly vertical. At this location,

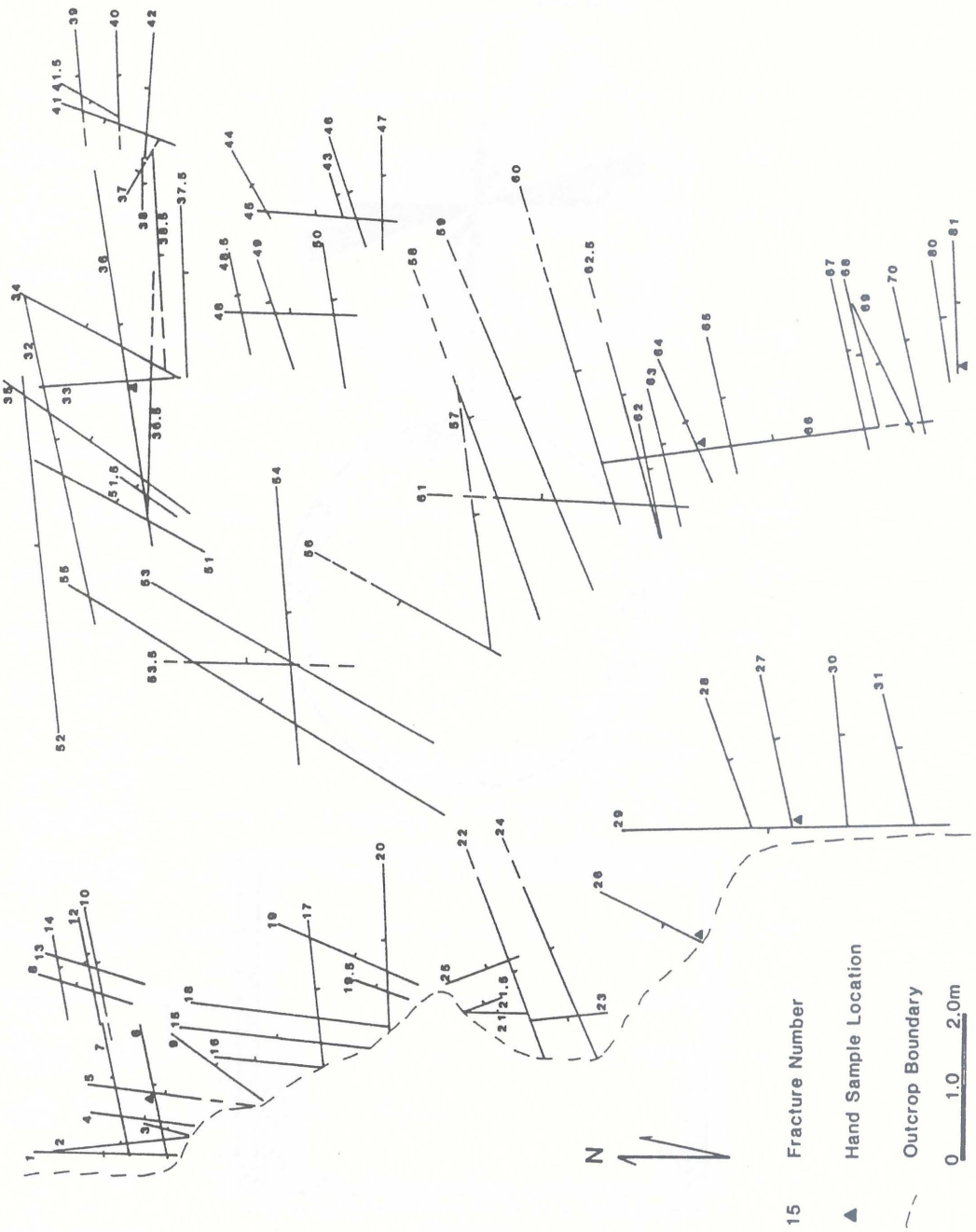

Figure 16: Results of fracture mapping at the Colorado Mesa 1 site.

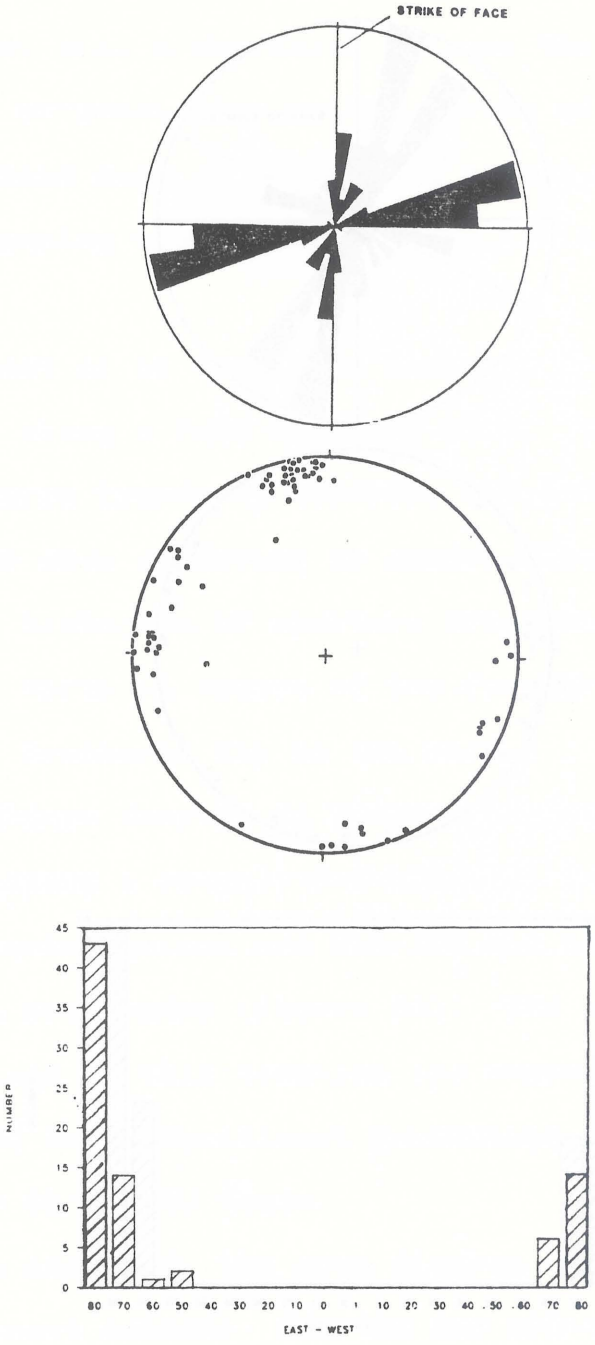

Figure 17: Rose diagram (top), stereonet (middle) and histogram (bottom) of fracture orientations and dips at the Colorado Mesa 1 site.

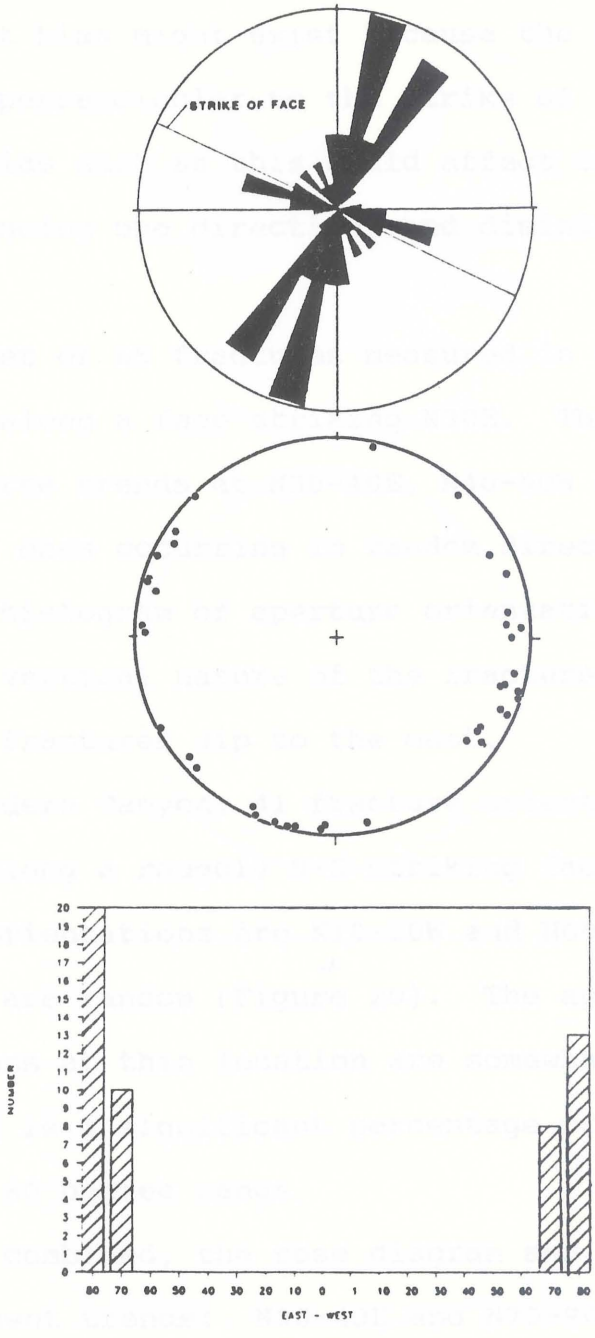

Figure 18: Rose diagram (top), stereonet (middle) and histogram (bottom) of fracture orientations and dips at the Colorado Mesa 2 site.

an apparent bias might exist because the fractures are generally perpendicular to the strike of the outcrop face. A bias such as this could affect the combined data, enhancing one direction, and diminishing the others.

The set of 65 fractures measured in Closed Canyon was taken along a face striking N30E. The fractures exhibit three trends at N30-40E, N40-50W and N70-80W, with minor ones occurring in random directions (Figure 19). The histogram of aperture orientations once again shows the vertical nature of the fractures, and also that more fractures dip to the east.

In Madera Canyon, 41 fracture orientations were obtained along a roughly N-S striking face. Two major fracture orientations are N10-20W and N60-70W. Other fractures are random (Figure 20). The aperture orientations at this location are somewhat anomalous in that there is a significant percentage of fractures in the 70 to 80 degree range.

When combined, the rose diagram and stereonet show two prominent trends: N30-40E and N70-90E (Figure 21). These two trends are the likely result of conjugate faulting caused by the large scale Basin and Range

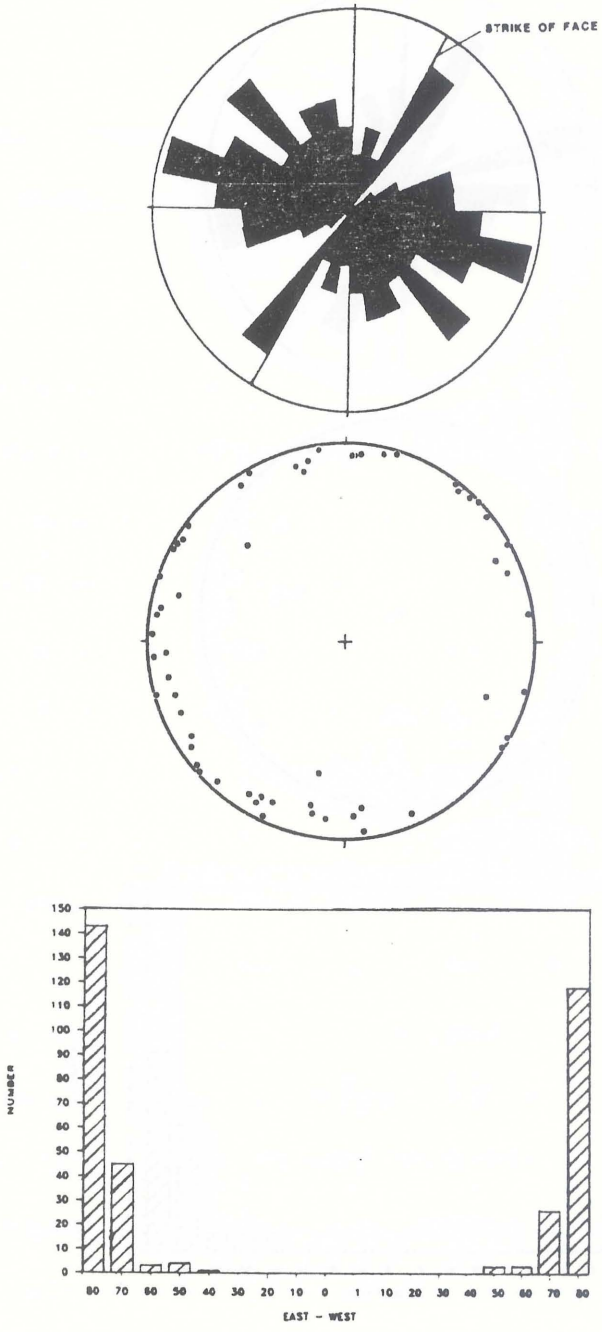

Figure 19: Rose diagram (top), stereonet (middle) and histogram (bottom) of fracture orientations and dips at the Closed Canyon site.

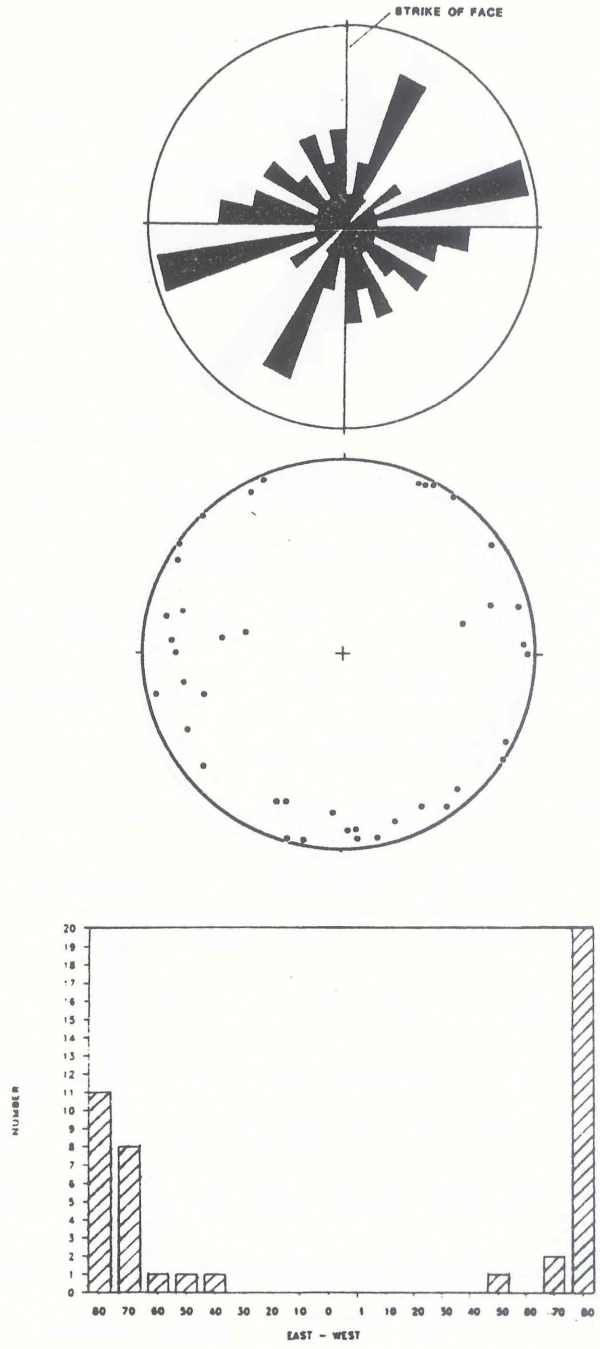

Figure 20: Rose diagram (top), stereonet (middle) and histogram (bottom) of fracture orientations and dips at the Madera Canyon site.

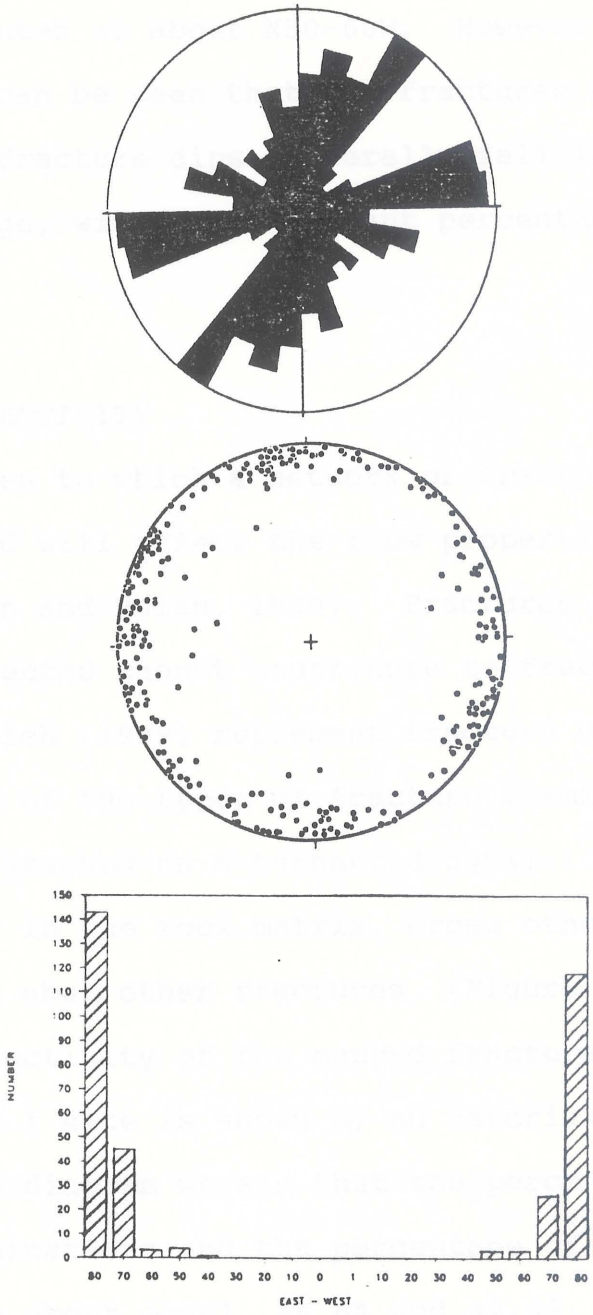

Figure 21: Rose diagram (top), stereonet (middle) and histogram (bottom) of fracture orientations and dips of the combined sites.

faulting oriented at about N50-60W. However, from the stereonet it can be seen that the fractures cover all directions. Fracture dips generally fall in the 80 to 90 degree range, with a significant percentage dipping to the east.

FRACTURE CONNECTIVITY

The degree to which a network of fractures is interconnected will affect the flow properties of a system (Barton and Hsieh, 1989). Fractures that are not interconnected cannot contribute to fracture flow. Barton and Hsieh (1989) represent fracture connectivity by the ratios of the types of fracture termination or interaction, graphed on a ternary diagram. Fractures may terminate in the rock matrix, cross other fractures, or abut other fractures (Figure 22).

The connectivity of the mapped fractures at the Colorado Mesa 1 site is shown by an asterisk in Figure 23. From the diagram we see that the percentage of fracture terminations and the percentage of fracture crossings are about equal, 44.6% and 42.3%, respectively. There are relatively few abutting fractures (13.1%).

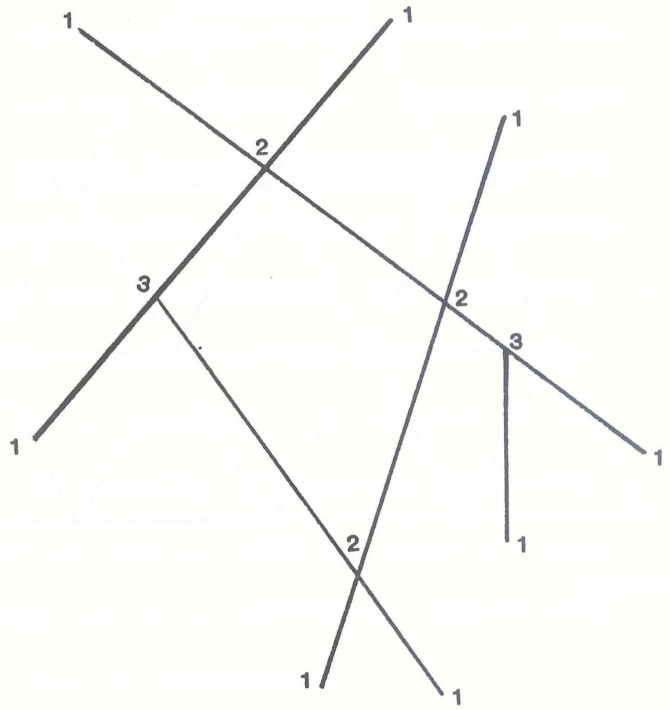

Figure 22: Sketch of types of fracture terminations:
1. blind, 2. crossing, 3. abutting.

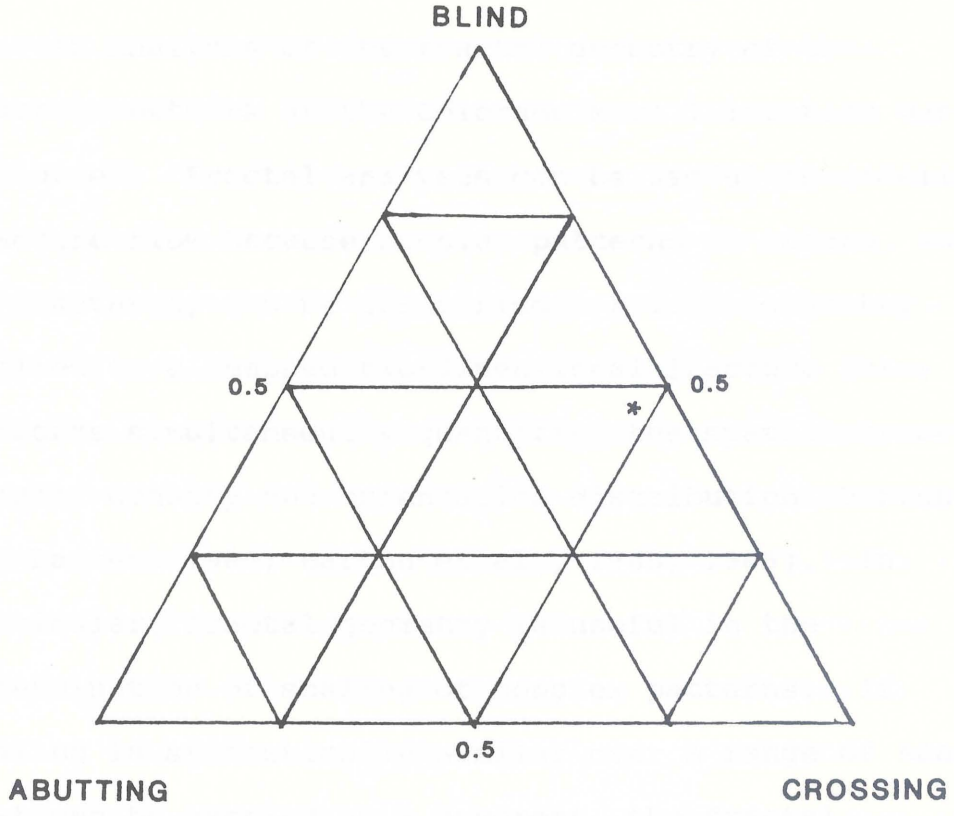

Figure 23: Ternary diagram of percentages of fracture intersections and terminations for the Colorado Mesa 1 site.

FRACTAL ANALYSIS

An analysis of the fractal geometry of the fracture network at the Colorado Mesa 1 location was performed. Fractal analyses can be useful in modeling fracture flow because complex patterns in nature, such as fractures, can be quantified. Fractal geometry applied to a mapped two-dimensional fracture trace networks simultaneously quantifies the spatial trace length, density and orientation distribution (Barton and Larsen, 1985; Barton et al., 1985, 1986). In particular, fractal geometry is useful in the determination of scaling of complex patterns. If scaling is statistically similar over a range of scales that can be sampled on a pavement, the fractal dimension, D, can be determined.

The procedure followed here is the box method, where grids of various sized square elements are successively placed over the maps. The number of elements containing a fracture trace are counted. The equation for the fractal distribution of lines on a map is

$$N\, r^{D} = 1$$

or equivalently,

$$D = \log N / \log (1/r)$$

where N = number of elements containing fracture traces, r = length of the side of the element, and D = the slope of the graphed line. The element size (r) is limited by two factors: 1) the smallest element should be no smaller than the shortest fracture, and 2) the largest element size should be smaller than the size at which all cells are occupied. The log of 1/r is plotted vs. log N for each cell size. The slope of the resulting line is D, and when D = 1, it is the fractal dimension of a straight line and when D = 2, it is the dimension of a filled plane. If the plot is fitted by a smooth line (straight or curved), the network is fractal over the range of r sampled. And if the line is straight, the network is scale independent over the range.

For the Colorado Mesa 1 site, a 12 by 10 meter area was mapped. Grid sizes started at 0.5 meters and went up to 3 meters. Table 2 gives the values for r and their corresponding N values. Figure 24 is a log-log plot, with a slope of 1.44. Therefore, the fractal dimension, D, lies somewhere between the straight line and the filled plane dimension. Because the plot is fitted by a smooth line, the fractures are fractal from 0.5 to 3.0 meter range. However, because each outcrop

Table 2: Values for r and N from the fractal analysis

r	N	log r	log N
0.5	334	0.300	2.52
0.6	245	0.220	2.39
0.7	194	0.150	2.29
0.8	171	0.097	2.23
0.9	146	0.046	2.16
1.0	129	0.000	2.11
1.2	101	-0.080	2.00
1.4	71	-0.150	1.85
1.6	62	-0.200	1.79
1.8	51	-0.255	1.71
2.0	44	-0.300	1.64

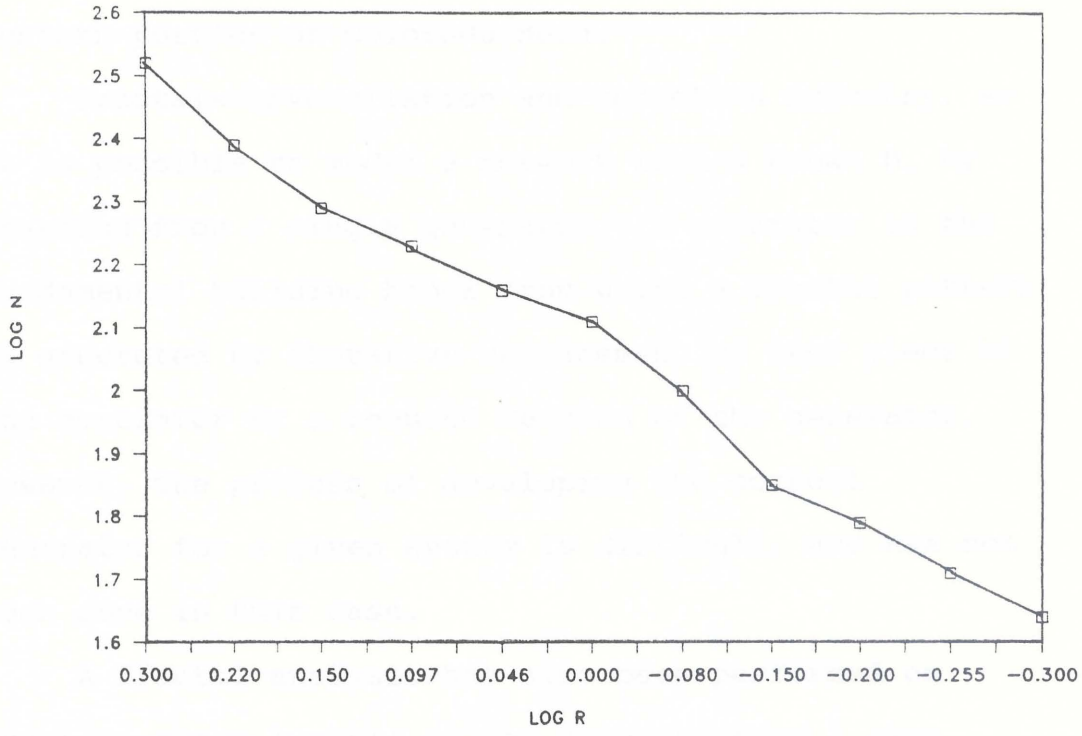

Figure 24: Fractal plot for fracture networks mapped on the Colorado Mesa 1 site.

lies on different fault blocks with the Santana Tuff, this analysis is probably only applicable to the western portion of Colorado Mesa.

Fractals have dilation and reduction symmetry, so it is possible to model a network with a known D, by starting from a single generator. A generator is the fundamental building block from which a fractal pattern is generated by iterative replacement of each piece of the generator by a reduced version of the generator. However, the process of developing the correct generator for a given system is difficult, and has not been done in this case.

A fractal analysis has also been performed on fracture trace lengths at the Colorado Mesa 1 site. The equation

$$N\ r^{E} = 1$$

describes this situation, where N = the number of fractures greater than a given r, the fracture trace length E is the scaling exponent (Table 3). Once again, a plot is made of log N vs log r, and E is the slope of the line. A high exponent indicates a higher frequency of short trace lengths. However, the result in this case is a curved line, indicating that the length of the fracture is scale dependent (Figure 25).

Table 3: Values for r and N from the trace length fractal analysis.

r (m)	N	log r	log N
0.5	80	0.03	1.90
1.0	73	0.00	1.86
1.5	60	-0.18	1.78
2.0	39	-0.30	1.59
2.5	22	-0.40	1.34
3.0	18	-0.48	1.26
3.5	14	-0.54	1.15
4.0	9	-0.60	0.95
4.5	7	-0.65	0.84
5.0	3	-0.69	0.48

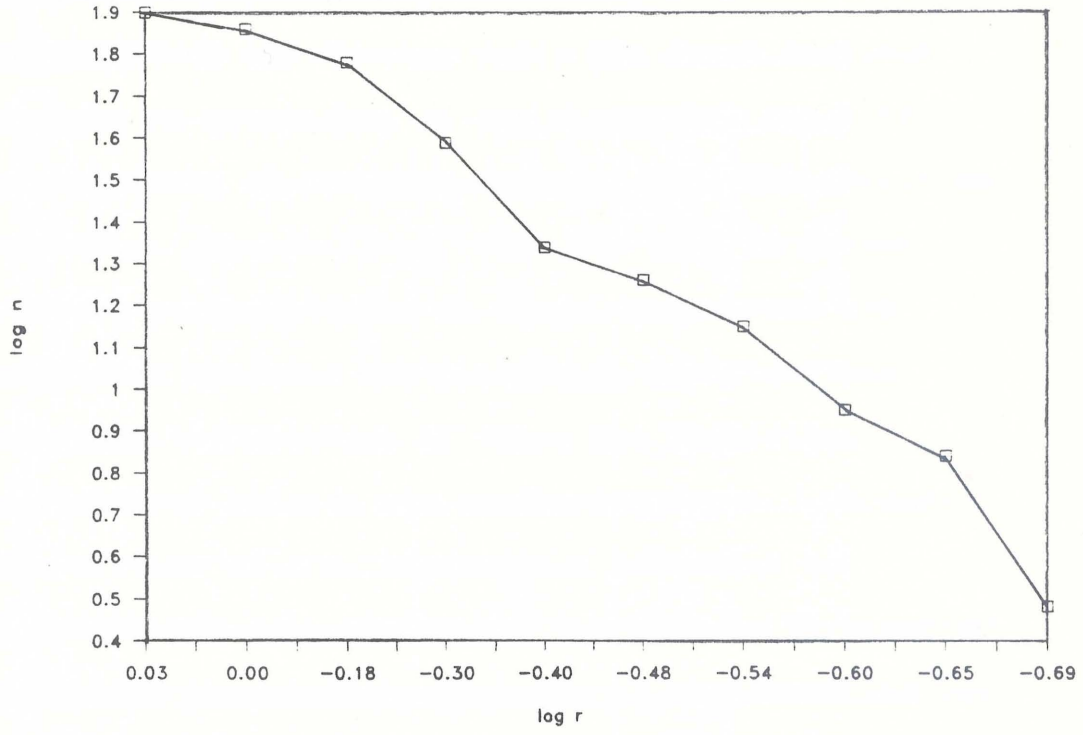

Figure 25: Fractal plot of frequency of trace lengths for the Colorado Mesa 1 site.

This means that if a larger area of the outcrop were mapped, the length of the fractures would have been longer, or visa-versa.

PERMEABILITY ANALYSIS

Two analyses of permeability patterns were performed on the Santana Tuff. The first analysis focused on weathering on the surface of the tuff, particularly of fracture surfaces, and the resulting effect on permeability. This was done by measuring surface permeabilities on fresh, weathered, and varnished surfaces and performing a statistical analysis to determine if there are significant differences between the weathering types. Secondly, the effects of flow emplacement direction on permeability were analyzed. The purpose in studying potential permeability patterns is to understand how they can affect fluid flow properties within the tuff.

These permeability measurements were obtained using an air minipermeameter. This permeameter was developed in the Petroleum Engineering department at the University of Texas at Austin. The prototype is described in Goggin, et al, 1988. Measurements were taken by recording the back pressure and percent flow of pressurized air forced into a rock. The back pressure and percent flow are converted to permeability in millidarcies.

EFFECTS OF WEATHERING

To determine the effects of weathering on permeability, 10 hand samples of the Santana Tuff, taken from each outcrop, were used. Each face of each sample was classified according to the degree of weathering: fresh, weathered, and varnished. Overall, 8 surfaces were weathered, 8 were varnished, and 2 were fresh.

VARNISHED SURFACES

A total of 372 permeability measurements were taken from varnished surfaces. A surface was classified as varnished if it exhibited an orange or black coating. These surfaces had been exposed to sunlight and wind. The mean permeability for a varnished surface is 3.31 md, roughly equivalent to 10^{-8} meters/sec, with a standard deviation of 1.72.

This data also appears to be lognormal, as can be seen in Figure 26. This histogram shows a typical lognormal distribution. We would expect such a lognormal distribution because the varnishing process has altered the rock to have many fine pores at the expense of the large pores. As the surface becomes more varnished, there will be a lower probability

VARNISHED SURFACES

```
Midpoint
  0.00   **
  1.00   **
  2.00   ****************************
  3.00   ************************
  4.00   *************
  5.00   ***
  6.00   ****
  7.00   **
  8.00   **
  9.00   *
 10.00   *
 11.00
 12.00   *
 13.00
 14.00
 15.00

 N = 373 (Each * represents 5 obs.)
```

Figure 26: Histogram of varnished surface permeabilities in millidarcies.

of hitting a large pore, which would result in a higher permeability. Nscore tests were performed which supports the lognormal distribution of varnished surface permeabilities (Figure 27)(Snedecor and Cochran, 1980; Ryan, et al, 1985). An Nscore test is a graphical technique used to determine whether a population is normal. The sample is plotted versus the values, on the average, of a normal population. If the plot is a straight line, the sample is from a normal population, but if the plot exhibits curvature, the population is not normal. The top graph in Figure 27 is a curved line, indicating that the data are not normal. The bottom graph is a plot of log permeability. Because the line is straight over most of the plot, the data can be considered lognormal.

Samples of varnished surfaces were examined under the SEM, XRD and in thin section. The SEM analysis indicated that the varnished surface exhibits a lamellate micromorphology as defined by Dorn (1986). This type of micromorphology is not unexpected because of the environment in which the Santana Tuff is located--vegetation cover is minimal. The SEM photos in Figure 28 indeed exhibit a lamellate texture.

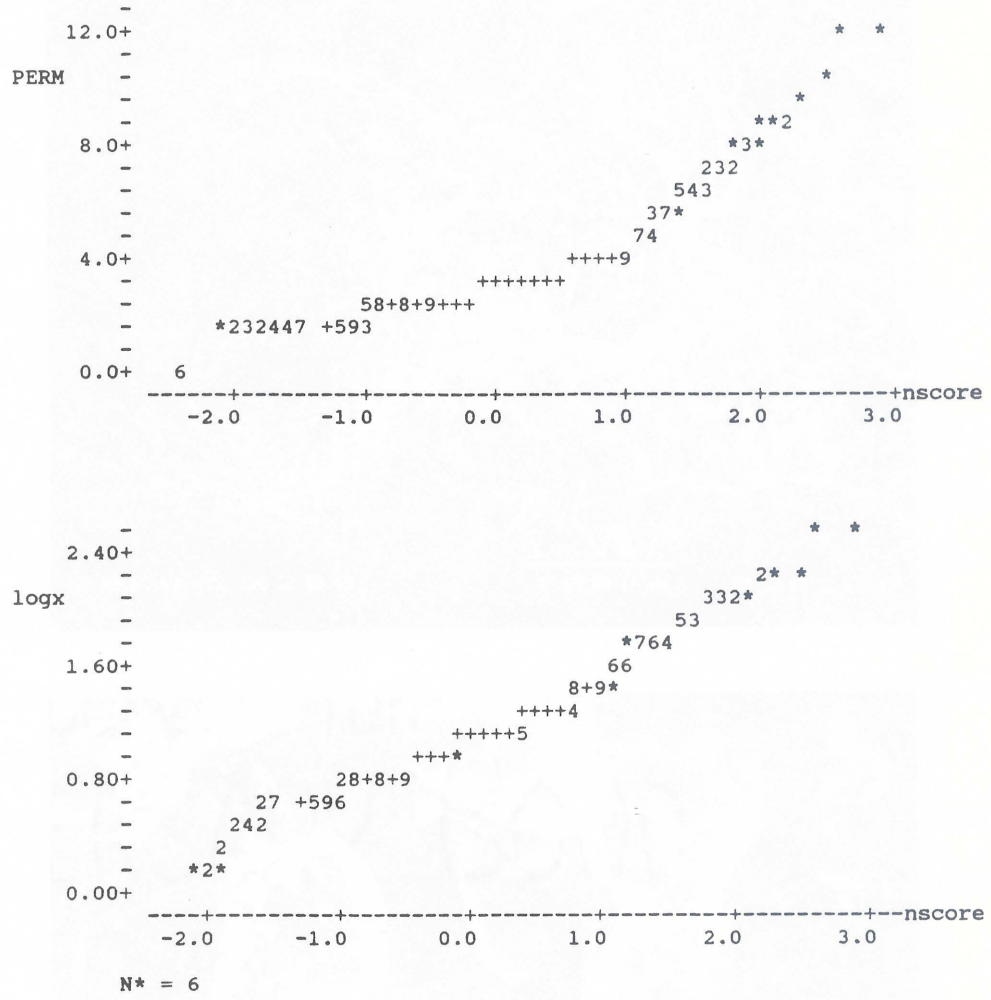

Figure 27: Results of the Nscore tests for varnished surface permeabilities (top), and for log varnished surface permeabilities (bottom).

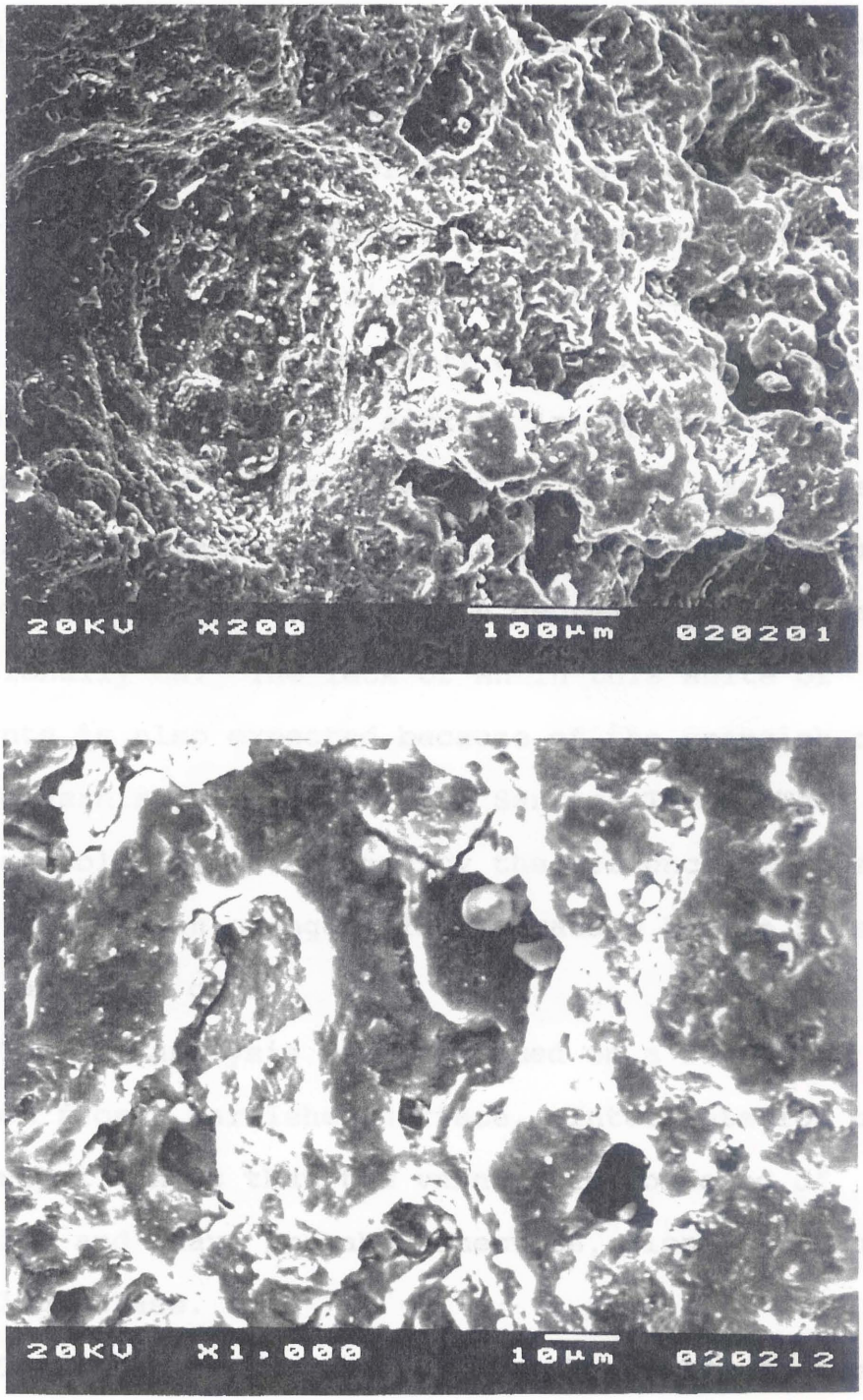

Figure 28: SEM photograph of a varnished tuff surface at a magnification of 200x (top) and 1000x (bottom).

These varnished surfaces are caused by the deposition of windblown clay particles. Occasionally at low magnification some microcracks can be seen, but these generally are more visible at higher magnification. Figure 29 shows such a microcrack at a high magnification. They generally are not continuous over the whole sample and are similar in appearance to mudcracks. EDS (element detection system) analysis of varnished SEM samples shows that the following elements are present: Si, Al, Fe, K, in decreasing order, and occasionally Ca. The lack of Mn in this suite of elements is also expected because of the orangish color of the varnish, typical of the Santana Tuff. The varnish color is determined by the presence or absence of Fe and Mn; an orange color is caused by the presence of Fe and lack of Mn.

The XRD analysis was performed on a sample scraped from a varnished surface. Interpretation of the output shows that the varnish is composed of hematite and clay, probably smectite, along with quartz and plagioclase.

Thin sections were made through samples of the Santana Tuff. In cross sections through the varnish, the thickness of the varnish can be measured.

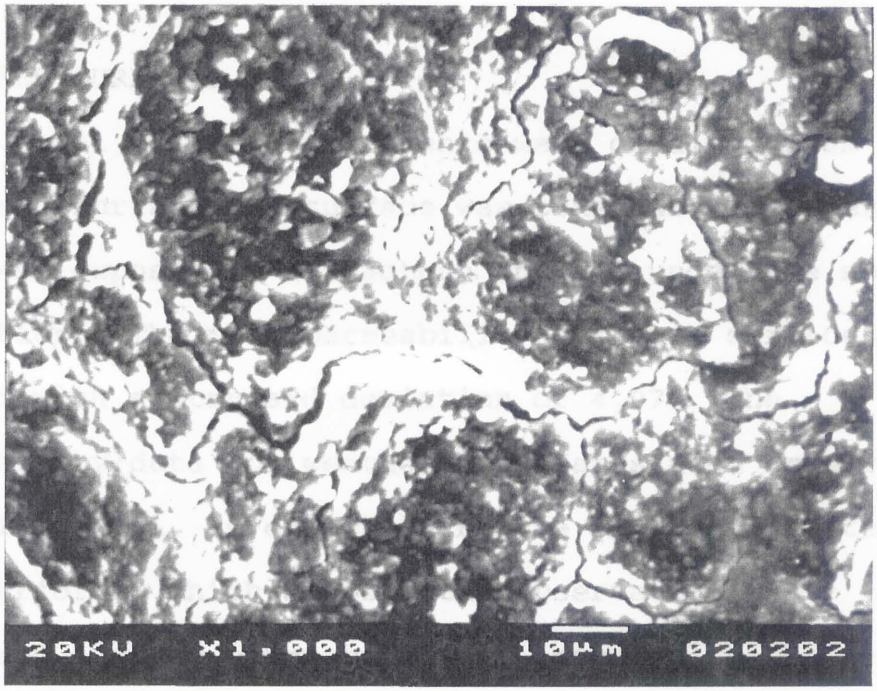

Figure 29: SEM photograph of a varnished tuff surface with microcracks at a magnification of 1000x.

Generally the varnish is about 0.05 mm to 0.1 mm thick, but it can also be up to 1.0 mm thick. Figure 30 compares the thin rind to the diffuse rind. The varnish may also be found filling in microcracks near the surface of the tuff.

WEATHERED SURFACES

A total of 452 measurements were obtained from weathered surfaces. A surface was considered weathered if it was exposed in a fracture and had undergone some alteration. The mean permeability for such surfaces is 5.03 md with a standard deviation of 4.07. The permeability data for weathered surfaces also appears to be lognormal, as expected (Figure 31). Nscore tests were performed which support the observation that weathered surface permeability is lognormally distributed (Figure 32).

Weathered tuffs were examined by SEM, XRD, and in thin section. The SEM analysis shows that the weathered surfaces are not much different in texture than varnished surfaces. At low magnification, the surface exhibits a lamellate micromorphology as a result of the deposition of clay particles (Figure 33). EDS analysis detected the following elements:

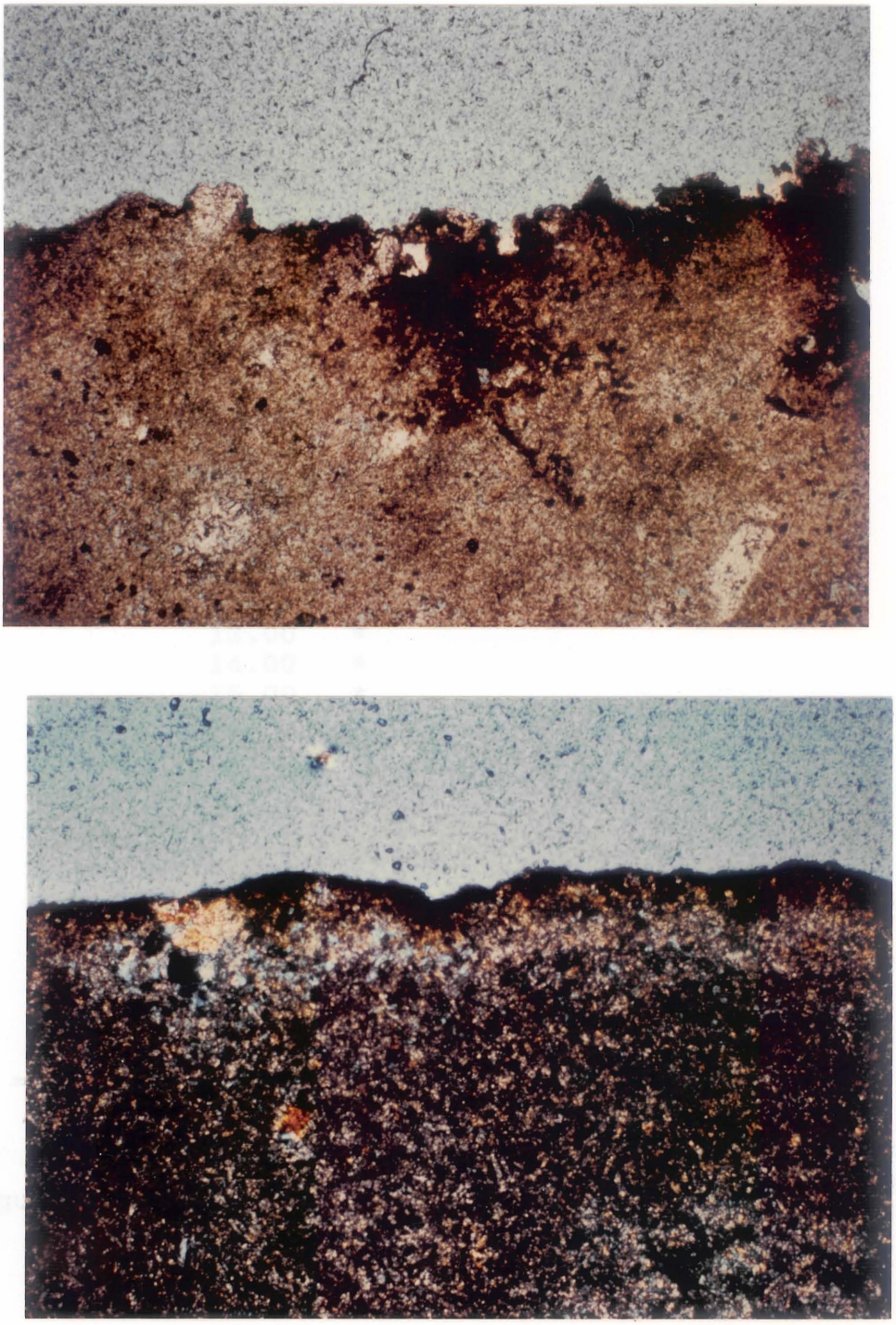

Figure 30: Photomicrographs of thin sections showing thick (top) and thin (bottom) varnishes.

WEATHERED SURFACES

```
Midpoint
    0.00   **
    1.00   **
    2.00   ********************
    3.00   ************************
    4.00   ************
    5.00   ******
    6.00   *******
    7.00   *****
    8.00   *** **
    9.00   ****
   10.00   *
   11.00   *
   12.00   **
   13.00   *
   14.00   *
   15.00   *
   16.00   *
   17.00   **
   18.00   *
   19.00   *
   20.00   *
   21.00
   22.00
   23.00   *
   24.00
   25.00
   26.00   *

N = 452 (Each * represents 5 obs.)
```

Figure 31: Histogram of weathered surface permeabilities in millidarcies

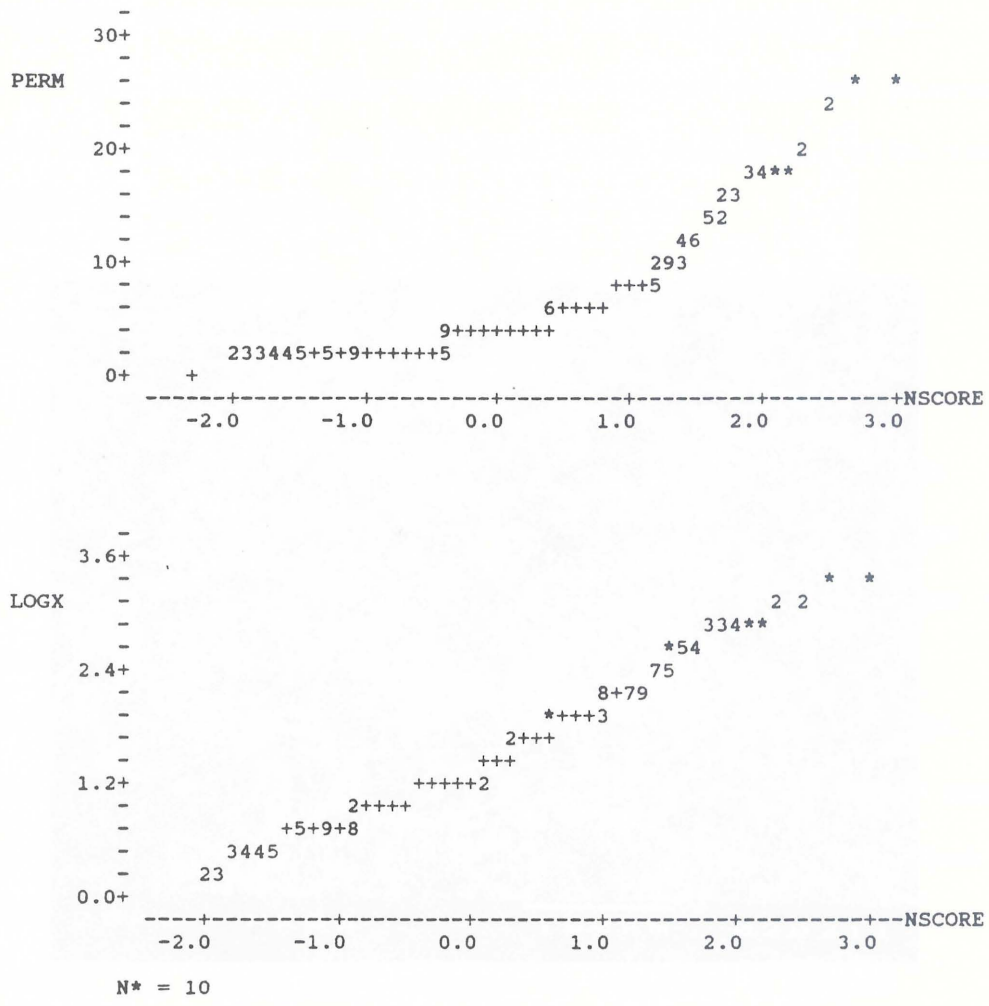

Figure 32: Results of the Nscore tests for weathered surface permeabilities (top), and for log weathered surface permeabilities (bottom).

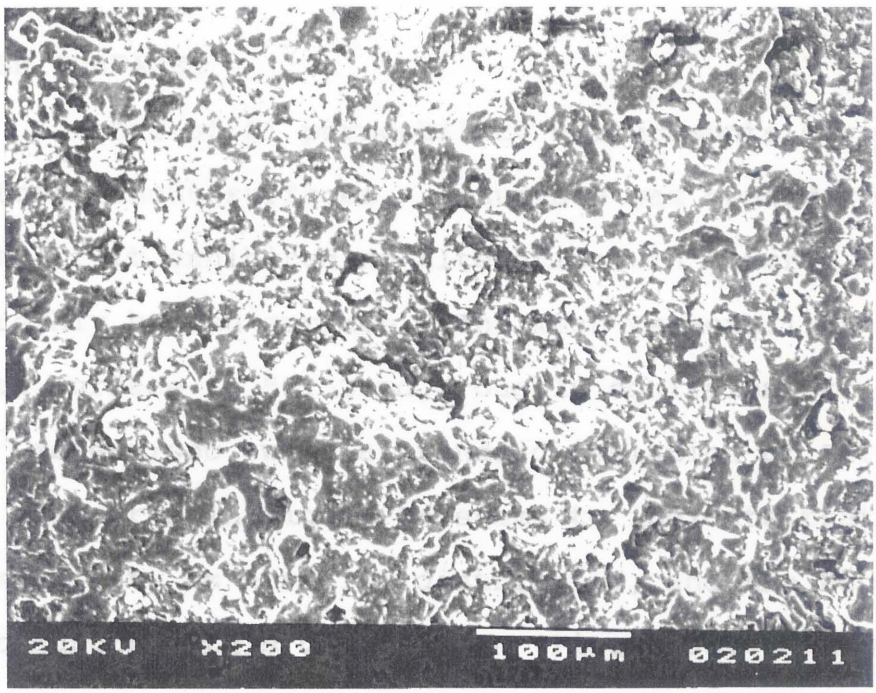

Figure 33: SEM photograph of a weathered tuff surface at a magnification of 200x.

result of the deposition of clay particles (Figure 33). EDS analysis detected the following elements: Al, Si, Fe, and occasionally Ca and K, in decreasing order.

The XRD analysis of the weathered surface showed the same minerals as the varnished analysis, with the addition of calcite.

FRESH SURFACES

A total of 81 permeability measurements were taken on fresh uncut surfaces. A surface was considered fresh if it exhibited no alteration. In general, it was a freshly broken surface. The mean permeability of a fresh surface is 55.33 md, roughly equivalent to 10^{-7} meters/sec, with a standard deviation of 22.51. The histogram in Figure 34 seems to indicate that the permeability is normally distributed, and the Nscore test supports this observation (Figure 35). We would expect the fresh tuff matrix to exhibit a normal distribution of permeability because of the distribution of pore sizes as well as the scale of the measuring device. The permeameter measures the permeability of fresh surfaces at a scale where most pores will appear to be the large at the scale of the

FRESH SURFACES

```
Midpoint
 10.00    **
 15.00    **
 20.00    ****
 25.00    ***
 30.00    ****
 35.00    ****
 40.00    ****
 45.00    *****
 50.00    ****
 55.00    *********
 60.00    ************
 65.00    *****
 70.00    **
 75.00    *****
 80.00    *****
 85.00    ****
 90.00    ***
 95.00    **
100.00
105.00
110.00    *
```

N = 81

Figure 34: Histogram of fresh surface permeabilities in millidarcies

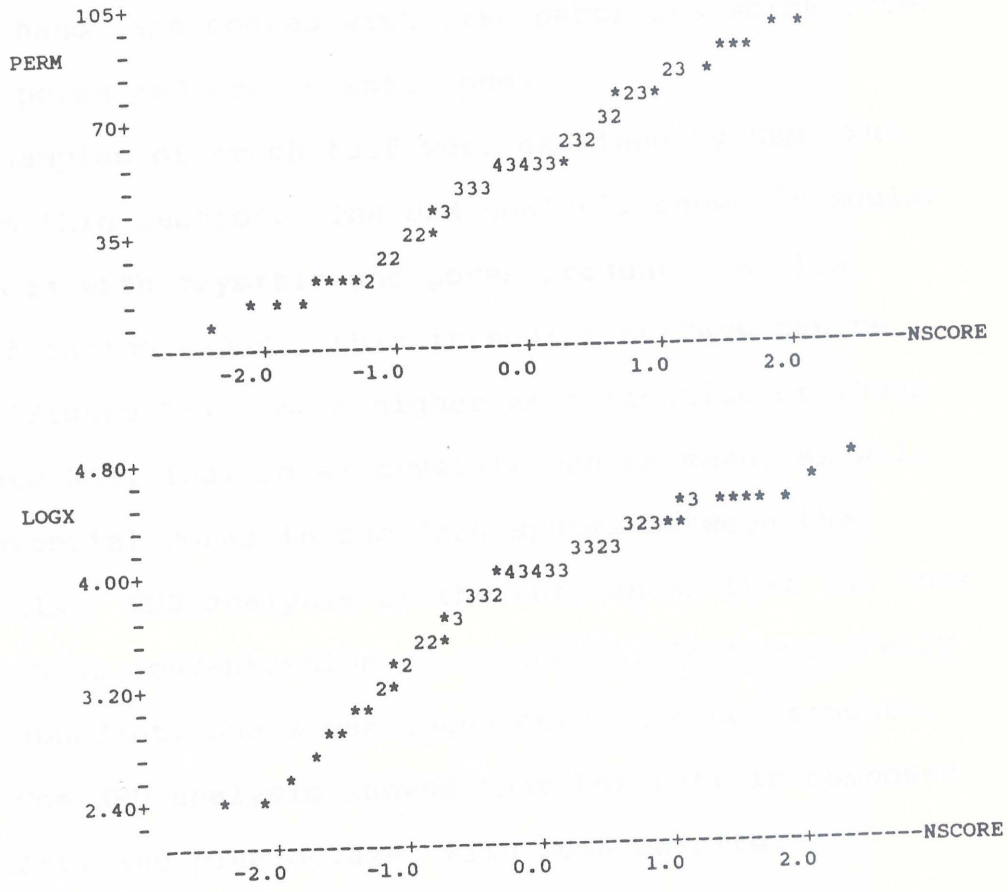

Figure 35: Results of the Nscore tests for fresh surface permeabilities (top), and for log fresh surface permeabilities (bottom).

permeameter. Varnished and weathered surfaces, on the other hand, are coated with clay particles which cover large pores and create small ones.

Samples of fresh tuff were examined by SEM, XRD, and in thin section. The SEM analysis shows irregular surfaces with crystals and pores present. At low magnification (200x), this irregular surface can be seen (Figure 36). At a higher magnification of 1000x (Figure 36), individual crystals can be seen, as well as potential pores in the dark spaces between the crystals. EDS analysis of the tuff shows that the rock has a high concentration of Al and Si, Fe is generally less abundant, and K was found only in minor amounts.

The XRD analysis showed that the tuff is composed of quartz and plagioclase, with some calcite. Examination of fresh tuffs in thin section showed typical glass shards in the ground mass, quartz and plagioclase phenocrysts and open pores.

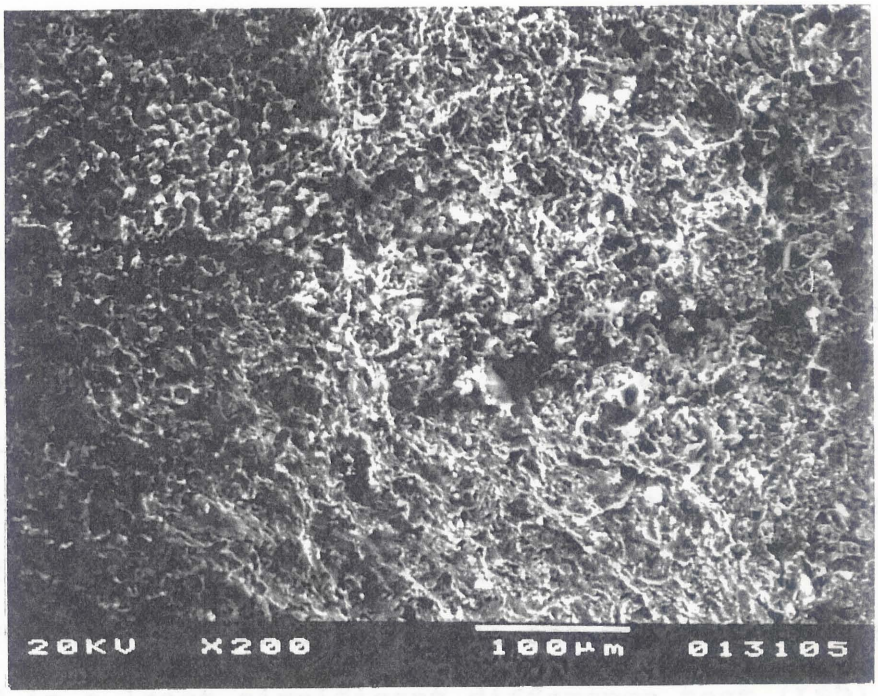

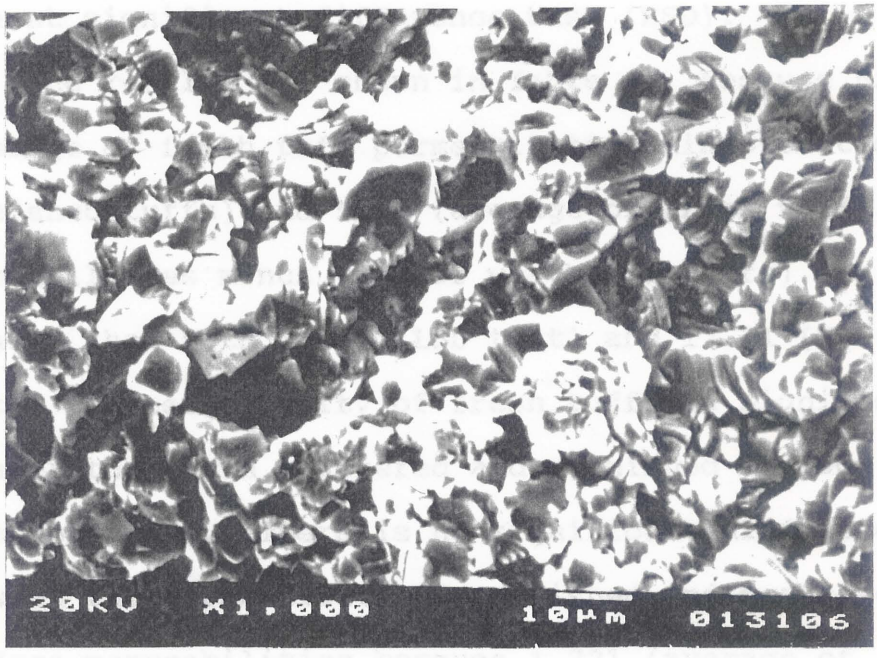

Figure 36: SEM photographs of a fresh tuff surface at a magnification of 200x (top), and 1000x (bottom).

COMPARISON OF WEATHERING EFFECTS

A one-way statistical analysis was performed on the permeability data. This analysis compares the means of several populations to determine whether significant differences exist between the populations (Snedecor and Cochran, 1980; Ryan et al., 1985). This test was performed on the permeabilities of fresh surfaces ("3"), weathered surfaces ("2"), and varnished surfaces ("1"), even though the distributions are different. The results of the one-way test were then used in a least significant difference test (LSD) and highest significant difference test (HSD).

The results are shown in Table 4. Because 52.01 (average of fresh tuff permeabilities minus that of varnished tuffs) and 50.3 (average of fresh tuff permeabilities minus that of weathered tuffs) are greater than both 14.45 (LSD test) and 17.31 (HSD test), the permeability of fresh tuffs is significantly greater than both weathered and varnished surface permeabilities. There is no significant difference between the permeability of varnished and weathered surface permeabilities because 1.721 (average of weathered tuff permeability minus that of varnished tuffs) is less than both the LSD and HSD tests.

ANALYSIS OF VARIANCE ON PERM

SOURCE	DF	SS	MS	F	p
weather	2	193037.0	96518.5	1774.03	0.000
ERROR	903	49128.9	54.4		
TOTAL	905	242165.9			

LEVEL	N	MEAN	STDEV	INDIVIDUAL 95 PCT CI'S FOR MEAN BASED ON POOLED STDEV
1	373	3.309	1.720	*)
2	452	5.030	4.073	*)
3	81	55.330	22.513	(*
				15 30 45

LSD AND HSD TESTS

	$-\overline{1}$	$-\overline{2}$
$\overline{3}$	52.01	50.3
$\overline{2}$	1.721	-
$\overline{1}$	-	-

$$s / n = (\text{MS error} / \text{DF weather})^{1/2} = 5.215$$

# of treatments	2	3
st. range*	2.77	3.32
signif. diff**	14.45	17.31
	LSD	HSD

* st. range from A14, p.480

** signif. diff = (s / n) (st. range)

Table 4: LSD and HSD tests from the one-way statistical analysis.

EFFECTS OF FLOW DIRECTION

An ash flow tuff is deposited as the result of a nueé ardente-type eruption. The resulting mix of gas and pyroclastic material flows over the ground. As it cools, the weight of the overlying material causes clasts to flatten. This aspect of the study deals with how permeability may vary with flow emplacement direction, as determined by direction of flattening. To accomplish this, three perpendicular sides were cut on tuff samples. Each side is either parallel or perpendicular flattening, and therefore flow direction. Because the Santana was deposited in a north-south direction, flattening occurred in the horizontal plane.

Sample 26 from the Colorado Mesa West site is shown in Figure 37. The direction of flattening and flow are easily seen in this picture. Two other samples were also prepared and examined in this manner, for a total of 266 measurements. The mean for permeability parallel to flattening is 25.00 md with a standard deviation of 23.09, for permeability perpendicular to flow emplacement, 19.64 md with a standard deviation of 17.07, a 27% decrease in permeability.

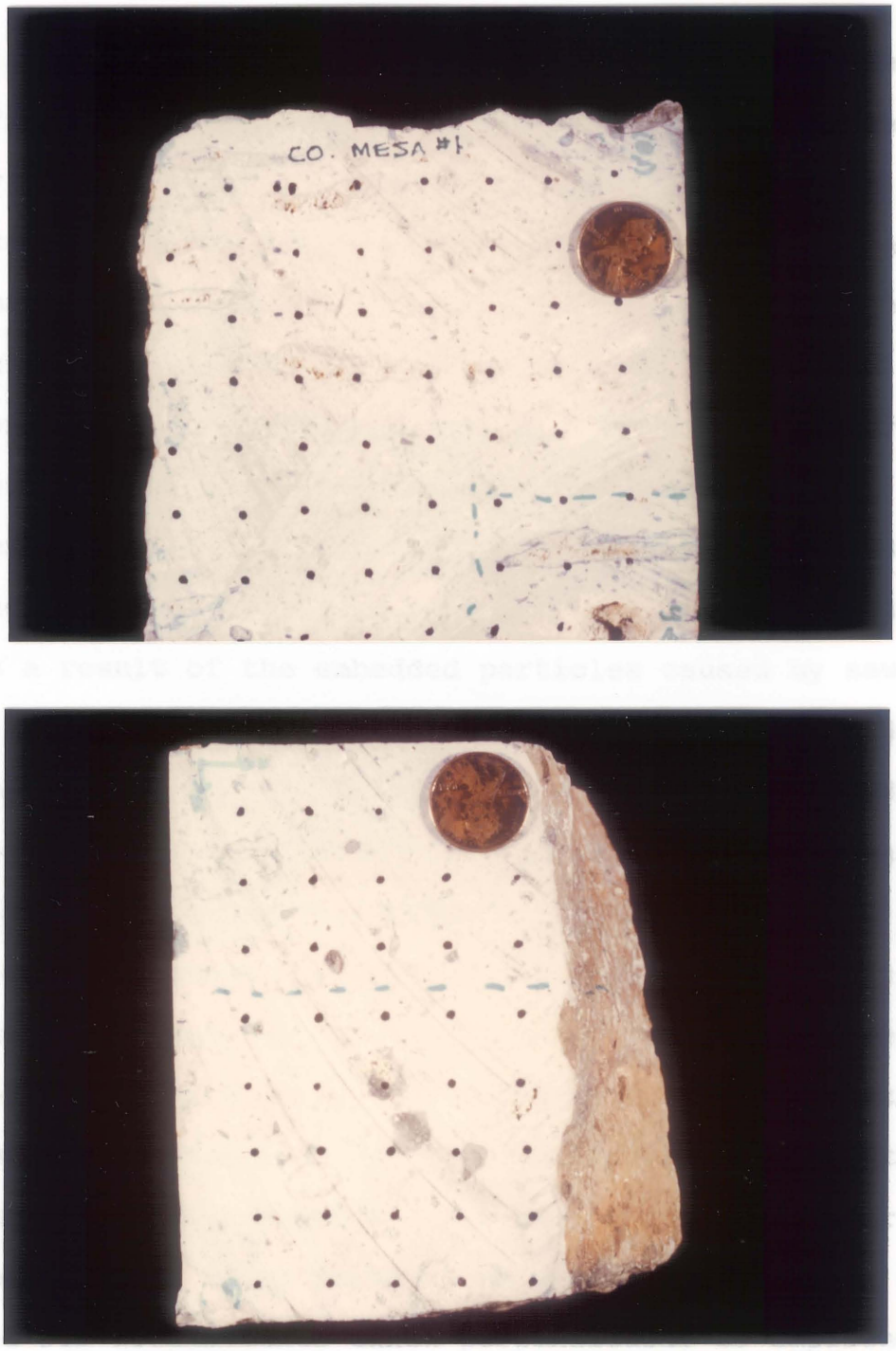

Figure 37: Photographs of cut sample 26 from Colorado Mesa 1 showing pumice fragments parallel (top) and perpendicular (bottom) to flow.

The cut surfaces were examined to determine the effects that sawing has on the rock. Striations caused by the saw blade are present on the surface, so it was examined in the SEM to see the effects of sawing on a small scale. It is evident that the surface of the tuff has been embedded with dust particles (Figure 38). For this reason, cut surfaces and fresh surfaces are not directly compared in this study. The permeabilities for fresh and cut surfaces are 55.33 md and 23.22 md, respectively. The decrease of over half is a result of the embedded particles caused by sawing.

Next, the weathered and varnished samples used in the weathering effects study were classified according to flow direction. The photograph from Figure 4 (page 14) shows how the flow direction can be determined by flattened pumice fragments. For weathered surfaces, it was found that the permeability parallel to emplacement had a mean of 5.48 md; permeability perpendicular to emplacement was 2.70 md. For varnished surfaces, the same trend was observed. The mean permeability for measurements taken parallel to emplacement is 3.44 md, and for measurements taken perpendicular to emplacement is 2.99 md. The permeability difference between parallel and perpendicular measurements is only 15%.

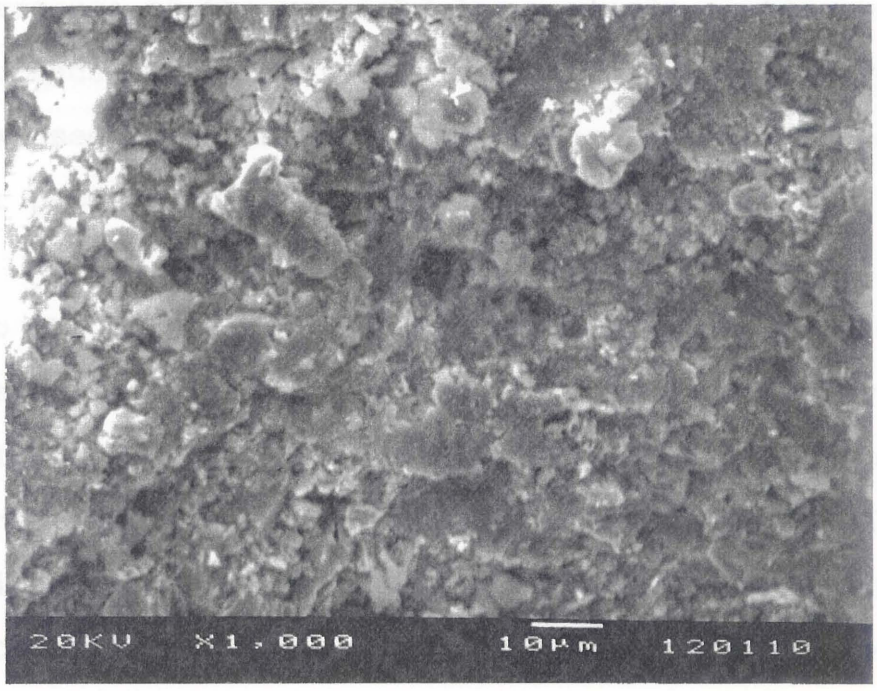

Figure 38: SEM photograph of a sawed tuff surface.

Table 5 contains a summary of the directional permeability data. No statistical tests were performed on these data. It is not surprizing that effects of flow emplacement direction would be minimized by the presence of the varnish/clay particle coating on the surface of the tuff. This coating tends to cover all exposed surfaces with clay particles, whether parallel or perpendicular to emplacement direction.

In a comparison of this surface permeability data to the core plug data from the Institute for Gas Technology, we see that the core plug data show significantly higher permeability (Table 1, page 31). There are two factors that may have contributed to this difference. First of all, the volume sampled in the core plug was larger, and preferred pathways for travel may have existed. Secondly, the core plugs were dried before measurement. Although the permeabilities are different, the pattern is the same. The permeabilities for cores 64B-3, parallel to emplacement, and 64C-4, perpendicular to emplacement, are 255.99 md and 116.89 md, respectively. This is a 46% decrease in permeability perpendicular to emplacement.

Table 5: Directional permeability statistics for fresh, weathered, and varnished surfaces.

SURFACE	DIRECTION	NUMBER	MEAN	STANDARD DEVIATION
fresh	parallel	81	55.33	22.51
	perpendicular	NA	NA	NA
cut	parallel	178	25.01	23.09
	perpendicular	88	19.64	17.07
weathered	parallel	379	5.48	4.29
	perpendicular	73	2.7	0.87
varnished	parallel	266	3.44	1.74
	perpendicular	106	2.99	1.63

(permeability in millidarcies)

In summary, the Santana Tuff was analyzed for fracture and permeability patterns. Fracture patterns were examined by analysis of fracture orientations at six outcrops of the Santana Tuff. Permeability patterns were examined from samples taken from each of the six outcrops. Over 1000 permeability measurements were examined for dependence on degree of weathering and/or direction of flow emplacement. The conclusions about these analyses are reviewed in the next section.

CONCLUSIONS

This study was an analysis of fracture and permeability patterns of the Santana Tuff. The fracture analysis consisted of determining the fracture patterns present, as well as a fractal analysis of a mapped outcrop. The permeability analysis consisted of three parts: the effects of weathering, the effects of flow direction, and the analysis of tuff samples by SEM, XRD, and thin section.

1. Fracture patterns: Fracture orientations were examined from six outcrops of the Santana Tuff. The strikes and dips were obtained at five outcrops by traversing the outcrop face. At the sixth outcrop the fractures were mapped. The fracture data were then plotted on stereonets and rose diagrams. It was found that the fractures are not randomly oriented at each outcrop. This may be due to tectonic influences, or the topography over which it was emplaced. It was also discovered that the fracture patterns vary significantly from outcrop to outcrop. Each of the outcrops were located on different fault blocks of the

Santana Tuff. The fractures do not appear to be predictable from the large scale to the small scale.

2. Fractal analysis: The analysis of fractal geometry at the Colorado Mesa 1 site showed two characteristics: (a) The slope of the line is 1.44, meaning that the fractal dimension lies between the straight line dimension and the plane dimension, (b) Because the plot is a smooth line, the fractures are fractal over the 0.5 to 3.0 meter range. The fracture trace length analysis indicates that the fracture trace lengths are scale dependent.

3. Weathering effects on permeability: Handsamples taken from each outcrop were classified according to the degree of weathering they exhibited. Fresh surfaces were generally broken from the outcrop. Weathered surfaces generally exhibit some degree of alteration and were exposed in fractures. Finally, those surfaces classified as varnished all exhibited an orange-black coating. Over 1000 measurements were obtained from the handsamples. The mean for fresh tuff permeability was 55.33 md, for weathered tuffs was 5.03 md, and for varnished tuffs was 3.31 md. The one-way

analysis shows that there is a significant difference between fresh tuff permeability and varnished and weathered surface permeabilities. Fresh tuffs are an order of magnitude more permeable than both varnished and weathered surfaces. No significant difference was shown to exist between varnished and weathered surface permeabilities.

4. Analysis of tuffs: The three surface types; fresh, weathered, and varnished, were examined in SEM, XRD, and in thin section to look at the changes caused by weathering. The SEM and XRD examinations showed the varnished and weathered surfaces are composed of a platy clay particle (smectite) and Fe-oxide (hematite) coating. The fresh surfaces were irregular, exhibiting open pores and crystal surfaces. In thin section, the weathering rind ranges from 0.05 mm to 1.0 mm.

5. Flow direction: The analysis of the effects of flow emplacement direction on permeability showed that permeability is enhanced parallel to the flow direction. From the analysis of permeability on cut surfaces, permeability perpendicular to emplacement was shown to be about 30% less than permeability

parallel to emplacement. This pattern is also present on weathered and varnished surfaces. Permeabilities on varnished surfaces perpendicular to flow are 15% less than permeability taken parallel to flow. The presence of the clay particle coating on the surface of the varnished tuffs would tend to decrease the enhanced permeability parallel to flow because the particles coat any exposed surface.

IMPLICATIONS FOR WASTE DISPOSAL

The objective of this study was to illustrate potential fracture and permeability patterns that may be present in an ash flow tuff. Although the Santana Tuff is very similar to the tuffs at the Yucca Mountain site, no direct conclusions should be drawn from this study about the suitability of the site as a potential repository for high level hazardous waste. Nonetheless, this analysis indicates that there are some patterns which might be found in other ash flow tuffs.

The fracture analysis of the Santana Tuff showed that fracture orientations are controlled by tectonic forces, as well as the cooling and welding processes. This means that the orientation of fractures in any ash flow tuff will partially be determined by tectonic influences of the area in which the tuff is found. Cooling fractures will however, be nearly vertical. And those fractures found in compound cooling units are continuous throughout the unit.

The permeability analysis showed that the presence of weathering on tuff surfaces decreases the surface permeability by an order of magnitude. The analysis of permeability dependence on direction of

flow emplacement found that tuffs have enhanced permeability parallel to emplacement.

A possible scenario for waste disposal, using the results of the Santana Tuff, is as follows. On the outcrop, during a large rainfall event, less water will be absorbed into the rock matrix, causing greater runoff into the fractures. Because the fractures are more continuous, water can penetrate deeper into the tuff. The vertical nature of the fracture would channel the waste straight down. This may indicate that water will reach the waste cannisters sooner than expected. If the waste has breached the cannisters, this low permeability barrier on the surface of fractures may also inhibit their absorption into the matrix. However, any water or radionuclides absorbed into the matrix will move laterally through the tuff because of the enhanced permeability in the same direction as flow emplacement.

REFERENCES

Allmendinger, R.W., 1987, Stereonet, vers ion 2.9, 29 p.

Arenal, C.R., 1964, Estudio geologico para localization de Yacimiento de carbon en la area Ojinga-San Carlos, Estado de Chihuahua, Mexico: Bolentin de la Asociacion Mexicana de Geologo Petroleros, v. 16, no. 5 and 6, p. 121-142.

Bourke, P.J., 1987, Channeling of flow through fractures in rock: Geoval, s. 2.5, 12 p.

Barker, D.F., 1983, Igneous Rocks: Prentice-Hall, Inc Englewood Cliffs, New Jersey, 417 p.

Barton, C.C., and Hsieh,P.A., 1989, Physical and hydrologic flow properties of fractures: Fieldtrip guidebook T385, 28th International Geological Congress, 36 p.

Barton, C.C., and Larson, E., 1985, Fractal geometry of two-dimensional fracture networks at Yucca Mountain, southwestern Nevada, in Fundamentals of Rock Joints: Proceedings of the International Symposium, Bjorkliden, Sweden, p. 77-84.

Barton, C.C., Larsen, E., and Baechle, P.E., 1985, Fractal Geometry of two-dimensional sections through fracture networks at Yucca Mountain, southern Nevada (abst): Eos, Transactions of the American Geophysical Union, v. 66, no. 46, p. 1089.

Barton, C.C., Page, W.R., and Larsen, E., 1986, Pattern of development of fracture networks (abst): Geological Society of America, Abstracts with Programs, v. 18, no. 6, p. 536.

Berry, L.G., Mason, B., and Dietrich, R.V., 1983, Mineralogy: W.H. Freeman and Company, San Francisco, 561 p.

Cook, E.F., 1960, Great Basin ignimbrites, in: Guidebook to the Geology of East Central Nevada, Boettcher, J.W. and Sloan, W.W., eds., p. 134-141.

Chuchula, R.J., 1981, Reconnaissance geology of the Sierra Rica area, Chihuahua, Mexico: University of Texas unpublished Master's thesis.

Degraff, J.M., and Aydin, A., 1987, Surface morphology of columnar joints and its significance to mechanics and direction of growth: Geological Society of America Bulletin, V. 99, p. 605-617.

Dorn, R.I., 1986, Rock Varnish as an indication of aeolian environmental change, in: Aeolian Geomorphology, Nickering, W.G., ed., p. 291-307.

Dorn, R.I., 1984, Cause and implications of rock varnish microchemical laminations: Nature, v. 310, p. 767-770.

Dorn, R.I., and Oberlander, T.M., 1982, Rock varnish: Progress in Physical Geography, v. 6, p. 317-367.

Duguid, J.O. and Lee, P.C.Y., 1977, Flow in fractured porous media: Water Resources Research, v. 13, p. 558-566.

Goggin, D.J., Thrasher, R.L., and Lake, L.W., 1988, A theoretical and experimental analysis of minipermeameter response including gas slippage and high velocity flow effects: Insitu, p. 79-116

Gregory, J.L., 1981, Volcanic stratigraphy and K-Ar ages of the Manuel Benavides area, Northeastern Chihuahua, Mexico, and correlation with the Trans-Pecos volcanic province: University of Texas unpublished Master's thesis, 78 p.

Immitt, J.P., 1981, Skarn and epithermal vein mineralization in the San Carlos caldera region, northeastern Chihuahua, Mexico: Unpublished Master's thesis, University of Texas, 109 p.

Klavetter, E.A., 1984, An estimation of hydraulic properties of unsaturated, fractured rock: Sand84-2642, Sandia National Laboratories, Albuquerque, New Mexico.

Krumbein, W.E., and Jens, K., 1981, Oecologia, Berlin, v. 50, p. 25.

Long, J.C.S., Remer, J.S., Wilson, C.R., and Witherspoon, P.A., 1982, Porous media equivalents for networks of discontinuous fractures: Water Resources Research, v. 18, no. 3, p. 645-658.

Maxwell, R.A., and Dietrich, J.W., 1970, Correlation of Tertiary rock units, West Texas: Bureau of Economic Geology Report of Investigations #70.

McKnight, J.F., 1968, Geology of the Bofecillos Mountains area, Trans-Pecos Texas: University of Texas Ph.D unpublished dissertation.

McKnight, J.F., 1970, Geology of the Bofecillos Mountain area Trans-Pecos Texas: Bureau of Economic Geology, University of Texas at Austin, Geologic quadrangle map no 37, 36p.

Moench, A.F., 1984, Double porosity models for a fissured ground water reservoir with fracture skin: Water Resources Research, v. 20, no. 7, p. 831-846.

Moench, A.F., 1983, Analysis of constant discharge wells in fissured formations with fracture skins: Eos, Transactions, American Geophysical Union, v. 64, no. 18, p. 228.

Montazer, P., and Wilson, W.E., 1984, Conceptual hydrologic model of flow in unsaturated zone, Yucca Mountain, Nevada: U.S. Geological Survey, Water-Resources Investigation Report 84-4345.

Mualem, Y., 1976, A new method for predicting the hydraulic conductivity of an unsaturated fractured rock mass: Water Resources Research, v. 12, no. 3, p. 513-522.

Neuzil, C.E., Tracy, J.V., 1981, Flow through fractures: Water Resources Research, v. 17, p. 191-199.

Neretnieks, I., 1987, Channeling effects in flow and transport in fractured rocks--some recent observations and models: Geoval, s. 3.6, 21 p.

Peters, R.R., and Klavetter, E.A., 1988, A continuum model for water movement in an unsaturated fractured rock mass: Water Resources Research, v. 24, no. 3, p.416-430.

Peters, R.R., Klavetter, E.A., Hall, I.J., Blair, S.C., Heller, P.R., and Gee, G.W., 1984, Fracture and matrix hydrologic characteristics of tuffaceous materials from Yucca Mountain, Nye County, Nevada: SAND84-1471, Sandia National Laboratories, Albuquerque, New Mexico.

Peterson, D.W., 1979, Significance of flattening of pumice fragments in ash flow tuffs: Geological Society of America Special Paper 180, p. 195-204.

Ragan, D.M., and Sheridan, M.F., 1972, Compaction of the Bishop Tuff, California: Geological Society of America Bulletin, v. 83, p. 95-106.

Ross, C.S., and Smith, R.L., 1961, Ash flow tuffs--Their origin, geologic relations and identifications: U.S. Geological Professional Paper 366, 81 p.

Ryan, B.F., Joiner, B.L., and Ryan, T.A., 1985, Minitab Handbook, PWS-Kent Press, 385 p.

Schwartz, F.W., Smith, L., Crowe, A.S., 1983, A stochastic analysis of macroscopic dispersion in fractured media: Water Resources Research, v. 19, no. 5, p. 1253-1265.

Sinnock, S., Lin, Y.T., and Brannen, J.P., 1984, Preliminary bounds on the expected postclosure performance of the Yucca Mountain Repository Site, Southern Nevada: SAND84-1492, Sandia National Laboratories, Albuquerque, New Mexico.

Smith, R.L., 1960, Zones and zonal variations in welded ash flow tuffs: U.S. Geological Society Professional Paper 354-F, p. 149-159.

Smith, R.L., and Bailey, R.A., 1966, The Bandilier Tuff, a study of ash flow eruption cycles from zoned magma chambers: Bulletin of Volcanology, v. 29, p. 83-104.

Snedecor, G.W., and Cochran, W.G., 1980, Statistical Methods: Iowa State University Press, 507 p.

Soeder, D., 1989, personal communication.

Taylor-George, S, Palmer, F., Staley, J.T., Borns, D.J., Curtiss, B.J., and Adams, J.B., 1983, Fungi and bacteria involved in desert varnish formation: Microbial Ecology, v. 9, p. 227-245.

Thordarson, W., 1983, Geohydrologic data and test results from well J-13, Nevada Test Site, Nye County, Nevada: U.S. Geological Survey open File Report 84-149, Denver, Colorado, 28 p.

Waddell, R.K., Robison, J.H., and Blankennagel, R.K., 1984, Hydrology of Yucca Mountain and vicinity, Nevada-California--Investigative results through mid-1983: U.S. Geological Survey Water-Resources Investigations Report 84-4267, Denver, Colorado.

Wang, J.S., and Narasimhan, T.N., 1984, Hydrologic mechanisms governing fluid flow in a partially saturated, fractured porous tuff at Yucca Mountain: LBL-18473, Lawrence Berkeley Laboratory, Berkeley, California.

Winograd, I.J., 1971, Hydrogeology of ash flow tuffs: A preliminary statement: Water Resources Research, v. 7, no. 4, p. 994-1006.

Winograd, I.J., Thordarson, W., and Young, R.A.., 1971, Hydrogeology of the Nevada Test Site and vicinity: U.S. Geological Society Open File Report, 429 p.

Wolleben, J.A., 1966, Biostratigraphy of Ojinaga and San Carlos formations of west Texas and northeastern Chihuahua: unpublished Ph.D dissertation, University of Texas at Austin, 62 p.

Wood, W.W. and Fernandez, L.A., 1988, Volcanic rocks: The Geology of North America, v. o-2, Hydrogeology, p. 353-365.

VITA

Carla Marie Matherne was born in Galiano, Louisiana, on March 10, 1964, to Judith Reed and Robert Matherne. After attending Mt. Carmel Academy and Ben Franklin High School in New Orleans, she graduated from Kingwood High School, Kingwood, Texas, in 1982. She entered the University of Texas in the fall of 1982 and graduated with highest honors in the fall of 1986. For the spring of 1987 she was employed at Hall Southwest Water Consultants, Inc., as a geologist. In the fall of 1987 she entered the Graduate School of the University of Texas at Austin and was appointed to the Department of Energy's Radioactive Waste Management Fellowship. A summer practicum was performed at DOE-Headquarters in Washington, D.C., in 1989.
On August 11, 1990 she married Jeffrey Alan Fuller.

Permanent address: 3122 Village Park
Kingwood, Texas 77339

This thesis was typed by Carla Marie Matherne.